Journal of
Medicinal Chemistry

Article

Structure-activity Relationship of SPOP Inhibitors Against Kidney Cancer

Ze Dong, Zhen Wang, Zhong-Qiang Guo, Shouze Gong, Tao Zhang, Jiang Liu, Cheng Luo, Hualiang Jiang, and Cai-Guang Yang

J. Med. Chem., **Just Accepted Manuscript** • DOI: 10.1021/acs.jmedchem.0c00161 • Publication Date (Web): 16 Apr 2020

Just Accepted

is published by the American Chemical Society. 1155 Sixteenth Street N.W., Washington, DC 20036

Structure-activity Relationship of SPOP Inhibitors Against Kidney Cancer

Ze Dong,[†,§] Zhen Wang,[¶,†,§] Zhong-Qiang Guo,[Δ,#] Shouzhe Gong,[†] Tao Zhang,[†] Jiang Liu,[#] Cheng Luo,[†,‡] Hualiang Jiang,[†,‡,Σ] Cai-Guang Yang[†,‡,*]

[†] State Key Laboratory of Drug Research, Shanghai Institute of Materia Medica, Chinese Academy of Sciences, Shanghai 201203, China

[¶] College of Pharmacy, Nanjing University of Chinese Medicine, Nanjing 210023, China

[Δ] Department of Urology, Zhongnan Hospital of Wuhan University, Hubei 430071, China

[#] CAS Key Laboratory of Genome Sciences and Information, Beijing Institute of Genomics, Chinese Academy of Sciences, Beijing 100101, China

[‡] School of Pharmaceutical Science and Technology, Hangzhou Institute for Advanced Study, UCAS, Hangzhou 310024, China

[Σ] Shanghai Institute for Advanced Immunochemical Studies, ShanghaiTec University, Shanghai 201210, China

Keywords:

cytoplasmic SPOP, inhibitor, protein-protein interaction, ccRCC, kidney cancer

ABSTRACT

Speckle-type POZ protein (SPOP) is overexpressed in the nucleus and misallocated in the cytoplasm in almost all the clear-cell renal cell carcinomas (ccRCC), which leads to kidney tumorigenesis. Previously, we elucidated that the oncogenic SPOP-signaling pathway in ccRCC could be suppressed by **6b** that inhibits SPOP-mediated protein interactions. Herein, we have established a structure-activity relationship for **6b** analogs as SPOP inhibitors. Compound **6lc** suppresses the viability and inhibits the colony formation of ccRCC cell lines driven by cytoplasmic SPOP, superior to **6b**. Compound **6lc** binds to SPOP protein *in vitro*, and disrupts SPOP binding to PTEN in HEK293T cells, which causes the observable phenomena: a declined in the ubiquitination of PTEN, elevated levels of both PTEN and DUSP7, and decreased levels of phosphorylated AKT and ERK when ccRCC cell lines are exposed to **6lc** in a dose-response manner. Taken together, compound **6lc** is a potent candidate against kidney tumorigenesis.

INTRODUCTION

Kidney cancer is resistant to chemotherapy in clinic and usually metastasizes once the disease has already been diagnosed. Several drugs have been approved for the targeted therapy of kidney cancers.[1] Typically, these drugs are either kinase inhibitors for vascular endothelial growth factor (VEGF) and platelet-derived growth factor (PDGF) receptors or inhibitors for the mammalian target of rapamycin (mTOR). Significantly, the first checkpoint inhibitor Nivolumab, a monoclonal

antibody targeting PD-1, was approved in clinic for renal cell carcinomas (RCC) therapy.[2] Bevacizumab, another monoclonal antibody targeting the VEGF receptor, also shows good antitumor activity in patients with metastatic RCC.[3] Recently, the small-molecule inhibitor PT2399 was shown to successfully disrupt the HIF 2α-Arant interaction and to suppress the progression of clear-cell RCC (ccRCC). PT2385, the analog of PT2399, has been approved for the clinical research.[4, 5] Although these anti-tumor drugs and candidates are available for the treatment of ccRCC, the dual challenges of low response rate and drugs resistance demand urgent exploration of untargeted targets and underexplored chemical spaces for targeted therapy of ccRCC.

The nuclear speckle-type POZ protein (SPOP) plays important roles within the ubiquitination machinery in cancers.[6-8] SPOP contains an *N*-terminal MATH domain ($SPOP^{MATH}$) for selectively binding to a substrate protein and a *C*-terminal BTB adaptor domain for E3 ubiquitin ligase recognition.[9-11] Remarkably, the E3 ligase adapter SPOP is overexpressed in 85% of kidney cancers; accumulation of dislocated SPOP in the cytoplasm occurs in nearly 100% of the two predominant forms of kidney cancer, namely primary and metastatic ccRCC.[12] The cytoplasmic SPOP serves as a regulatory hub in order to promote cancer through the ubiquitination and degradation of multiple cancer proteins that are involved in cellular proliferation and apoptosis.[13] The two tumor suppressors, phosphatase-and-tensin homolog (PTEN) and dual-specificity phosphatase 7 (DUSP7) are central to the mechanism in the oncogenic SPOP-signaling. Binding of SPOP to PTEN and DUSP7 in the cytoplasm

degrades these two proteins, which inactivates its downstream AKT/ERK signaling pathways, and which eventually promotes ccRCC tumorigenesis. Indeed, the biological rationale is compelling, since the inhibition of SPOP-mediated protein interactions and the stabilization of PTEN and DUSP7 proteins would be beneficial for the treatment of ccRCC.

We have established that small-molecule targeting of the E3 ligase adaptor SPOP could be a specific approach against ccRCC.[14] Compounds **6a** and **6b** block the interaction of the SPOP ubiquitin ligase with its substrates (Figure 1), thus leading to the impaired proliferation of ccRCC cell lines that characteristically have cytoplasmic SPOP. Our discovery of compound **6b** convincingly demonstrates on a biochemical level in cells the therapeutic potential of blocking SPOP activity to stabilize PTEN and DUSP7 in order to suppress the AKT- and ERK-driven cancer-signaling pathways, which serves as "proof-of-principle" in order to manipulate the "undruggable" E3 ligase in the ubiquitin-proteasome system in ccRCC.[15, 16]

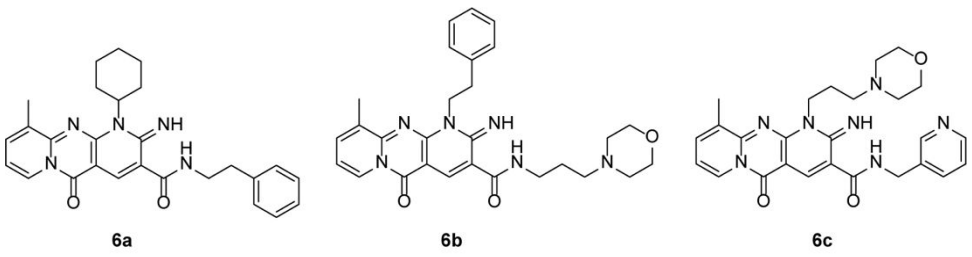

Figure 1. Structures of our previously reported SPOP inhibitors. Compound **6c** is a negative control.

In this study, we explored more chemical spaces and attempted to establish a structure-activity relationship (SAR) in the aspect of medicinal chemistry for SPOP

inhibitors. Several analogs of **6b** are shown to suppress the proliferation of ccRCC cell lines typically with single-digital micro-molar IC_{50} values. Among them, compound **6lc** is active against kidney cancer cell lines through the inhibition of the SPOP-mediated ubiquitination-signaling pathway in ccRCC.

RESULTS AND DISCUSSION

Chemical Synthesis. We performed structural optimization based on chemical scaffold of the established SPOP inhibitors in several aspects using medicinal chemistry strategy,[17, 18] including 1) *N*-substituents, 2) various amide side-chains, 3) the impact of methyl group position, 4) carboxylic acids and esters, and 5) conjugation shrinking (Figure 2).

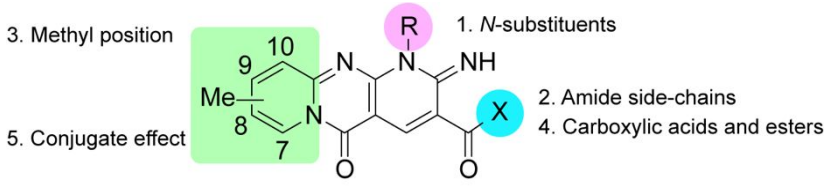

Figure 2. Design of different sets of SPOP inhibitors.

First, we investigated the effects of various *N*-substituents attached to cyclic amidine. Scheme 1 shows the synthetic route for compounds **6d-6z**. Condensation of 3-methylpyridin-2-amine **1** and diethyl malonate at elevated temperature provides 2-hydroxy-9-methyl-4H-pyrido[1,2-a]pyrimidin-4-one **2**. Simultaneous chlorination and formylation of **2** give the intermediate **3** under Vilsmeier-Haack reaction. Various imines **4** are obtained in good yields by treating the intermediate **3** with corresponding amines in the presence of anhydrous Na_2SO_4 in EtOH at room

temperature (rt). Lastly, refluxing imines **4** with α-cyanoacetamide **5a** in $CHCl_3$ provides a series of target compounds **6d-6z** in high yields.

Scheme 1. Synthesis of compounds **6d-6z**[a]

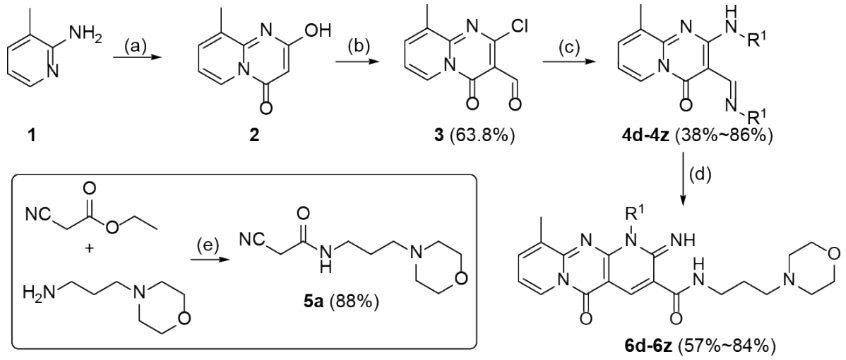

Compound	R^1	Compound	R^1	Compound	R^1
4d/6d	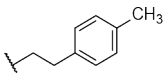	**4l/6l**	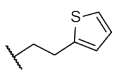	**4t/6t**	
4e/6e	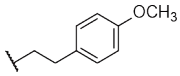	**4m/6m**	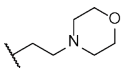	**4u/6u**	
4f/6f	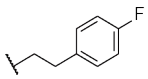	**4n/6n**	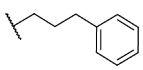	**4v/6v**	
4g/6g	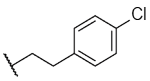	**4o/6o**	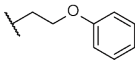	**4w/6w**	
4h/6h	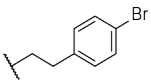	**4p/6p**	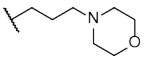	**4x/6x**	
4i/6i	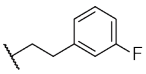	**4q/6q**	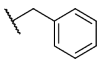	**4y/6y**	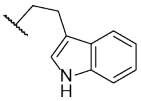
4j/6j	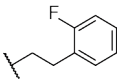	**4r/6r**	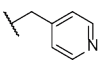	**4z/6z**	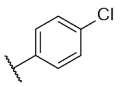
4k/6k	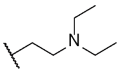	**4s/6s**			

[a] Reagents and conditions: (a) 220 °C, diethyl malonate, neat; (b) $POCl_3$, DMF; (c) R^1NH_2, Na_2SO_4, EtOH, rt, overnight; (d) **5a**, piperidine, $CHCl_3$, reflux, overnight; (e) neat, rt, 3 days.

Next, we introduced various amide sidechains into the main scaffold where the R^1 group is held constant as thiophenylethyl, because the sulfur-containing heterocycle

substituent might make the target compounds more “drug-like” and soluble. When α-cyanoacetamides **5b-5k** are employed as reagents in the one-step condensation with intermediate **4**, compounds **6la**-**6lj** are obtained in high yields (Scheme 2).

Scheme 2. Synthesis of compounds **6la-6lj**[a]

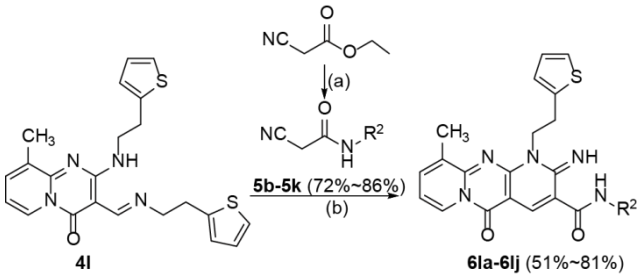

Compound	R^2	Compound	R^2
5b/6la	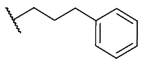	**5g/6lf**	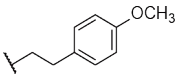
5c/6lb	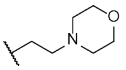	**5h/6lg**	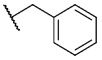
5d/6lc	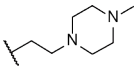	**5i/6lh**	
5e/6ld	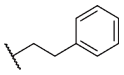	**5j/6li**	
5f/6le	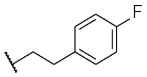	**5k/6lj**	

[a] Reagents and conditions: (a) R^2NH_2, neat, rt, 3 days; (b) piperidine, $CHCl_3$, reflux, overnight.

To investigate the impact of the methyl group attached to the planar tricycle (Figure 3), we synthesized 9-methyl substituted compounds **6lk** and **6ll** without methylation in a similar route for the synthesis of compounds **6la**-**6lj**.

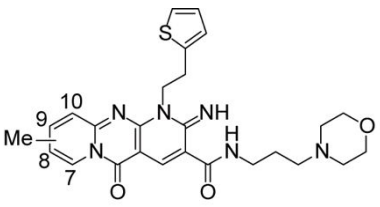

6l 10-Me
6lk 9-Me
6ll No-Me

Figure 3. Compounds with or without methyl group.

Furthermore, we prepared a set of esters **7a-7j** and the corresponding carboxylic acids **8a-8j** (Scheme 3). Ethyl esters **7** are synthesized in high yields through the reactions between compound **4** and ethyl α-cyanoacetate **5l**. Compounds **8a-8j** are obtained from alkaline hydrolysis of the corresponding ethyl esters **7a-7j**.

Scheme 3. Synthesis of compounds **7** and **8**[a]

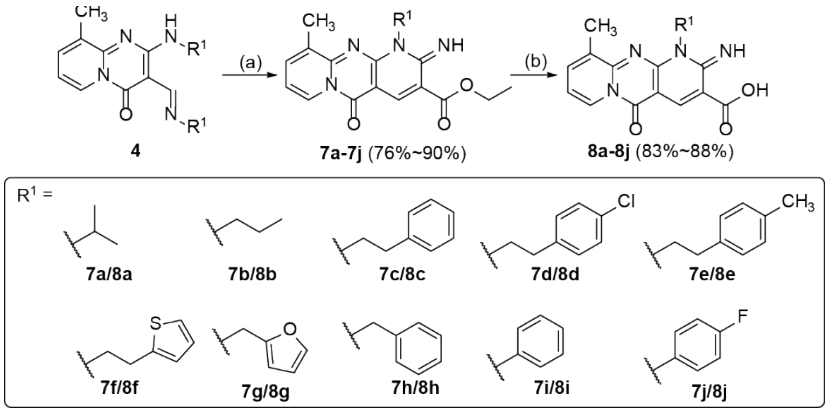

[a] Reagents and conditions: (a) ethyl α-cyanoacetate **5l**, piperidine, $CHCl_3$, reflux, overnight; (b) LiOH, THF/EtOH/H_2O, 45 °C, overnight.

Lastly, we synthesized several bicyclic compounds in order to investigate the effect of polycyclic conjugation on the inhibitory activity of SPOP inhibitors. The synthetic route for the preparation of compounds **13** and **14** is depicted in Scheme 4.[19, 20] Compound **9** is reacted with diethyl malonate to give ethyl ester **10**. Alkylation of **10** with (2-bromoethyl)benzene affords *N*-alkylated lactam **11**. Alkaline hydrolysis of **11** followed by condensation of carboxylic acids and amines provide target compound carboxamides **13** and **14** in high yields.

Scheme 4. Synthesis of compounds **13** and **14**[a]

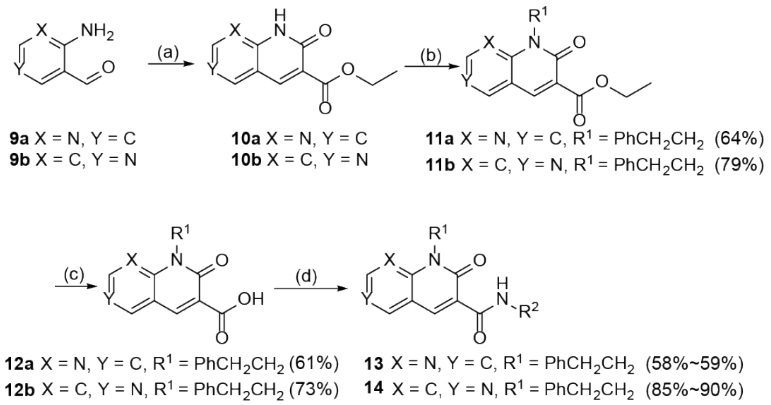

[a] Reagents and conditions: (a) piperidine, diethyl malonate, neat, reflux, overnight; (b) $PhCH_2CH_2Br$, K_2CO_3, DMF; (c) LiOH, THF/EtOH/H_2O, 45 °C, 4 hr; (d) R^2NH_2, HATU, DIEA, DMF.

Nano Differential Scanning Fluorimetry (nanoDSF) screening for SPOP binders. The nanoDSF assay that measures the thermal unfolding transitions (Tm) of an interested protein under native conditions, no extra dye is required.[21] In order to evaluate whether our newly synthesized compounds bind to SPOP protein *in vitro*, we performed a high-throughput screening for the Tm shift (*Δ*Tm) of $SPOP^{MATH}$ induced by compounds (Table 1 and S1). Several compounds could stabilize $SPOP^{MATH}$ protein with *Δ*Tm above 3.0 °C when the 10-fold compound was subjected to the nanoDSF assay, while compound **6c**, the negative control had minimal effect on the thermal stability of $SPOP^{MATH}$. To our delight, the *Δ*Tm could be further shifted up to 4.0 °C when the 20-fold compound **6b** was assayed. In addition to **6b**, compound **6e**, **6g-i**, **6l**, **6lc**, **6ld**, **7f**, and **8c** as listed in Table 1 stabilize $SPOP^{MATH}$ as showing *Δ*Tm values over 3.5 °C, alongside compounds **6r**, **6lf**, **6lj**, **7c**, and **8b** as shown in Table S1. Since the SPOP binder **6b** has been shown to be active against kidney cancer through targeting the SPOP-mediated signaling pathway in ccRCC, the nanoDSF assay could

be the first step of screening for small-molecule binders of SPOP that may be potential to inhibit SPOP-mediated protein interactions in the further biological annotation.

Table 1. Tm shift of $SPOP^{MATH}$ in the presence of compounds[a]

Compound	ΔTm (°C)		Compound	ΔTm (°C)	
	10 ×	20 ×		10 ×	20 ×
DMSO[b]	-1.7	-3.8	**6la**	2.8	2.6
6b	2.8	4.0	**6lb**	3.1	3.3
6c	0	0.2	**6lc**	3.1	3.5
6d	1.8	2.1	**6ld**	3.5	3.7
6e	2.5	3.6	**6li**	2.7	2.7
6f	2.5	2.9	**7d**	0.8	1.6
6g	2.4	3.5	**7e**	0.8	1.5
6h	2.3	3.5	**7f**	4.9	5.3
6i	3.7	5.3	**7j**	1.7	1.9
6l	3.2	5.1	**8c**	2.3	3.7

[a] Data was calculated using DMSO-treated $SPOP^{MATH}$ as the reference. [b] Data was obtained using naive $SPOP^{MATH}$ sample as the reference.

Antiproliferation of SPOP binders in ccRCC cell lines. Next, we performed an MTT assay in order to evaluate the antiproliferative effect of those SPOP binders identified in the nanoDSF screening on kidney cancer cells. The two ccRCC cell lines A498 and OS-RC-2 were assayed (Table S2). The known SPOP inhibitor **6b** was assayed as the positive control,[14] which inhibits the proliferation of A498 and OS-RC-2 cells up to 88% and 90% at 30 μM, respectively. Compound **6c**, the negative control minimally attenuates the proliferation of the two ccRCC cell lines at high concentrations. Several compounds, for example, **6d**-**6i**, **6k-6l**, **6n**, **6lc**, and **6li**, exhibited comparable antiproliferative activities with compound **6b**. Of note, those

compounds are SPOP binders too, which suggests that the nanoDSF is a validated assay for the initial screening of SPOP inhibitors.

Analysis of SARs. With these newly designed **6b** analogs in hand, we sought to analyze the SAR as of SPOP inhibitors. First, we investigated the effects of the R^1 substitutes on the inhibition of cell proliferation (Table 2). Introduction of methyl (**6d**), methoxyl (**6e**), fluoro (**6f**), chloro (**6g**), and bromo (**6h**) substitutes on the para-position of the phenethyl motif has negligible impacts on inhibitory activities, which display antiproliferative rates ranging between 88% and 97% against A498 and OS-RC-2 cells at 30 μM, comparable to compound **6b**. Interestingly, changing the position of fluoro group from the para-position (**6f**) or the meta-position (**6i**) to the ortho-position (**6j**) is unfavorable to the cell inhibitory activities, since the inhibitory rates of **6j** are decreased in both ccRCC cell lines. 2-(diethylamino)ethyl (**6k**) bearing an acyclic apolar substitute exhibits good cellular activity, with inhibitory rates of between 86% and 89% against the proliferation of A498 and OS-RC-2 cells, respectively. Compared to the thiophenylethyl-substituted compound **6l**, 2-morpholinoethyl-substituted analog **6m** exhibits declined inhibitory potency. 3-phenylpropyl-substituted compound **6n** largely suppressed cell proliferation, while an introduction of an oxygen atom into the chain of compound **6n** causes 2-phenoxyethyl-substituted compound **6o** to dramatically lose activity. Compound **6p** bearing 3-morpholinopropyl exhibits declined antiproliferative activities against both A498 and OS-RC-2. Compound **6q** with benzyl substituent exhibits declined activities, with 58% and 46% inhibitory rate against the proliferation of A498 and OS-RC-2 cells.

A similar phenomenon is observed on compound **6r** that having pyridin-4-ylmethyl group replaced benzyl substituent. Compounds **6s** and **6z** bearing aromatic groups exhibit attenuated antiproliferative activities against the two ccRCC cell lines, with inhibitory rates of 12% and 17% in A498 cells and 23% and 38% in OS-RC-2 cells, respectively. Compounds (**6t**, **6u**, **6v**, and **6w**) with the cyclic or linear R^1-substituted alkyl group also showed reduced inhibitory activity compared to **6b**. Lastly, the introduction of propargyl (**6x**) or the bulky indole (**6y**) proves unfavorable to antiproliferation. Taken together, results indicate that the introduction of polar substituents into the nitrogen is generally unfavorable to overall inhibitory potency in ccRCC cell lines.

Table 2. The SARs of *N*-substituents

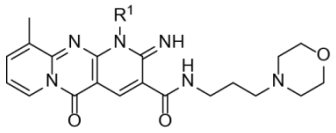

6b-6z

Compound	Inhibition @ 30 μM (%)		Compound	Inhibition @ 30 μM (%)	
	A498	OS-RC-2		A498	OS-RC-2
6b	88	90	**6o**	50	36
6d	91	94	**6p**	27	35
6e	90	88	**6q**	58	46
6f	90	88	**6r**	48	35
6g	90	97	**6s**	12	23
6h	89	96	**6t**	37	22
6i	89	92	**6u**	59	62
6j	61	74	**6v**	11	15
6k	86	89	**6w**	57	66
6l	90	82	**6x**	37	37
6m	35	40	**6y**	55	51
6n	90	91	**6z**	17	38

Next, we found that variations of amide sidechains in SPOP inhibitors have significant effects on the inhibition of proliferation in ccRCC cell lines (Table 3). Changing the 3-morpholinopropyl (**6l**) to the 3-phenylpropyl (**6la**) substituent reduces antiproliferative activities, with moderate inhibitory ratios of 62% and 58% for compound **6la** on A498 and OS-RC-2 cells at 30 μM, respectively. In general, compound **6lb**-**ld**, and **6lf** bearing the short amide sidechains largely retained their inhibitory activities against the proliferation of A498 cells. Surprisingly, compound **6le**, with 4-fluorophenethyl substituent, exhibits a significantly declined activity against proliferation, with inhibitory ratios of 12% and 21% for A498 and OS-RC-2 cells at 30 μM. The benzyl-amide substituted compound **6lg** also becomes less active. Of note, compounds **6lh** and **6li** with cyclic substituents largely maintain potency for inhibition, while the introduction of β-aminoalcohol (**6lj**) exerts only slight influence on antiproliferative activity.

Table 3. The SARs of amide sidechains

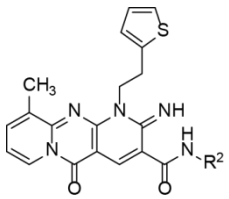

6la-6lj

Compound	Inhibition @ 30 μM (%)		Compound	Inhibition @ 30 μM (%)	
	A498	OS-RC-2		A498	OS-RC-2
6la	62	58	**6lf**	87	75
6lb	86	82	**6lg**	60	50
6lc	85	90	**6lh**	86	83
6ld	85	52	**6li**	90	90
6le	12	21	**6lj**	83	81

Subsequently, we investigated the impact of the methyl substituent on the planar tricycle. We compared the antiproliferative activities of compounds without the methyl group or with the methyl on different positions (Table 4). Compound **6lk** with 9-methyl substituent and **6ll** without methyl group showed attenuated activities against the proliferation compared with compound **6l** with 10-methyl substituent, thus indicating that the position of the methyl substituent in SPOP inhibitor is also important for the antiproliferation in ccRCC cell lines.

Table 4. The impact of methyl group

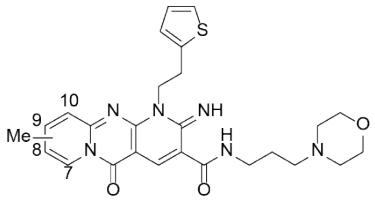

Methyl position	Compound	Inhibition @ 30 μM (%)	
		A498	OS-RC-2
10-Me	**6l**	90	82
9-Me	**6lk**	75	77
No-Me	**6ll**	62	56

As depicted in Table 5, most esters show reduced activities against the proliferation of A498 and OS-RC-2 cells compared to the corresponding amides (Table 2). Compound **7g** is the most active SPOP inhibitors among the 10 esters, but only achieves less than 60% antiproliferation in the two ccRCC cell lines at 30 μM. In addition, no carboxylic acids (**8a-j**), hydrolyzed from the corresponding esters (**7a-j**) under alkaline condition, show satisfied activities against ccRCC cell lines. In general, the esters or carboxylic acids as SPOP inhibitors are much less active than the amide derivatives.

Table 5. The SARs of esters and carboxylic acids

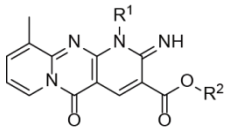

Compound	Inhibition @ 30 μM (%)		Compound	Inhibition @ 30 μM (%)	
	A498	OS-RC-2		A498	OS-RC-2
7a	27	23	**8a**	18	22
7b	38	35	**8b**	21	29
7c	24	20	**8c**	13	28
7d	42	48	**8d**	57	30
7e	51	49	**8e**	51	31
7f	38	49	**8f**	25	37
7g	59	56	**8g**	24	16
7h	24	26	**8h**	20	32
7i	51	10	**8i**	24	16
7j	33	16	**8j**	18	33

Lastly, in order to diversify the chemical scaffold of SPOP inhibitor, we shrank the tricyclic coplanar conjugation to the bicyclic system. We synthesized several bicyclic compounds with different substituents, including acids, esters, and amides (Table 6). Unfortunately, these bicyclic analogs usually display low antiproliferative activity in the two ccRCC cell lines, thus suggesting the important contribution of tricyclic coplanar conjugation on SPOP inhibitors.

Table 6. The SARs of planner conjugation

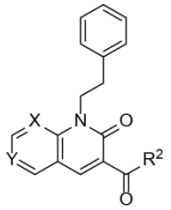

R^2	Compound X = N, Y = C	Inhibition @ 30 μM (%)		Compound X = C, Y = N	Inhibition @ 30 μM (%)	
		A498	OS-RC-2		A498	OS-RC-2
	**11a**	15	19	**11b**	14	15
	**12a**	33	24	**12b**	21	15
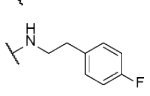	**13a**	8	14	**14a**	25	16

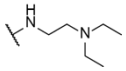	**13b**	13	30	**14b**	38	11

Quantitation of antiproliferative activity of SPOP inhibitors. Following the SARs analysis of SPOP inhibitors, we quantitatively determined the IC_{50} values for those compounds displaying >75% antiproliferative activities in both ccRCC cell lines at a single dose of 30 μM (Table 7). The IC_{50} of compound **6b** is 2.7 μM and 5.8 μM against A498 and OS-RC-2 cell lines, respectively, which is similar to our previously reported results. Compound **6c** is assayed as a negative control. In general, most tested compounds exhibited comparable activities to **6b** for the inhibition of ccRCC cell proliferation with single-digital micro-molar IC_{50} values, particularly those compounds containing apolar alkyl groups at the R^1-position. Compound **6d**-**6i** with phenethyl substitution, compound **6k** bearing acyclic 2-(diethylamino)ethyl sidechain, and compound **6l** containing heterocyclic substituent at the R^1 positions show comparable IC_{50} values to inhibitor **6b**. Similarly, compound **6n** with 3-phenylpropyl displays comparable activity to **6b**, while **6w** bearing the propyl group shows 2-fold drops in IC_{50} value for A498 cells. In line with the activities observed in single dosage MTT assay, the compounds bearing various amide sidechains also display potent antiproliferation against the two ccRCC cell lines, including **6lc**, **6lf**, and **6li**. Compound **6ld** is much less active against the proliferation in OS-RC-2 cells with an unknown mechanism.

Table 7. The antiproliferative activity of selected inhibitors

Compound	IC_{50} (μM)		Compound	IC_{50} (μM)	
	A498	OS-RC-2		A498	OS-RC-2
6b	2.7 ± 1.0	5.8 ± 1.2	**6k**	3.5 ± 0.7	3.9 ± 0.8

6c	> 50	> 50	**6l**	2.6 ± 0.5	7.6 ± 2.1
6d	2.1 ± 0.6	5.7 ± 1.2	**6n**	2.6 ± 0.2	5.1 ± 0.8
6e	2.8 ± 0.4	6.5 ± 1.1	**6w**	6.4 ± 0.9	5.2 ± 0.6
6f	3.1 ± 0.8	6.6 ± 1.0	**6lc**	2.1 ± 0.7	3.5 ± 0.5
6g	2.3 ± 0.3	4.0 ± 0.8	**6ld**	5.0 ± 1.3	24.2 ± 2.8
6h	3.0 ± 0.5	5.0 ± 1.0	**6lf**	2.8 ± 0.7	4.2 ± 0.7
6i	2.4 ± 0.4	4.6 ± 0.6	**6li**	6.3 ± 0.5	5.9 ± 0.8

Investigation of antiproliferative selectivity of 6lc. Although SPOP localizes in the nucleus and SPOP mutations are common in a variety of cancers, the ccRCC cell lines are unique in that overexpression of SPOP leads to ectopic localization in the cytoplasm. To this end, the SPOP inhibitor could selectively attenuate proliferation in ccRCC cell lines, but not in cell lines in which SPOP is absent from the cytoplasm. As expected, **6lc** displays antiproliferation in the two ccRCC cell lines of A498 and OS-RC-2 with IC_{50} of 2.1 μM and 3.5 μM, respectively (Figure 4A), while **6lc** minimally inhibits the growth of the non-tumor kidney cell line HK-2 (human proximal tubule epithelial cell line). In our SAR exploration, compound **6lc** is not sharply different from **6h** and **6lf** and our previously reported **6b** in potency against the proliferation of ccRCC cell lines (Table 7). These inhibitors also had similar thermal effects on the stabilization of SPOP protein *in vitro* (Table 1). However, the solubility of **6lc** is determined to be >90 μM in cell culture medium in the presence of 0.2% DMSO, which is much more soluble than **6b** (30-45 μM), **6h** (5-10 μM), and **6lf** (2.5-5 μM). In addition, **6lc** significantly inhibited the colony formation for both A498 and OS-RC-2 cells, superior to **6b**, **6h**, and **6lf** (Figure 4B). Taken these data together, we chose **6lc** as the representative inhibitor of SPOP-protein interaction for further investigations.

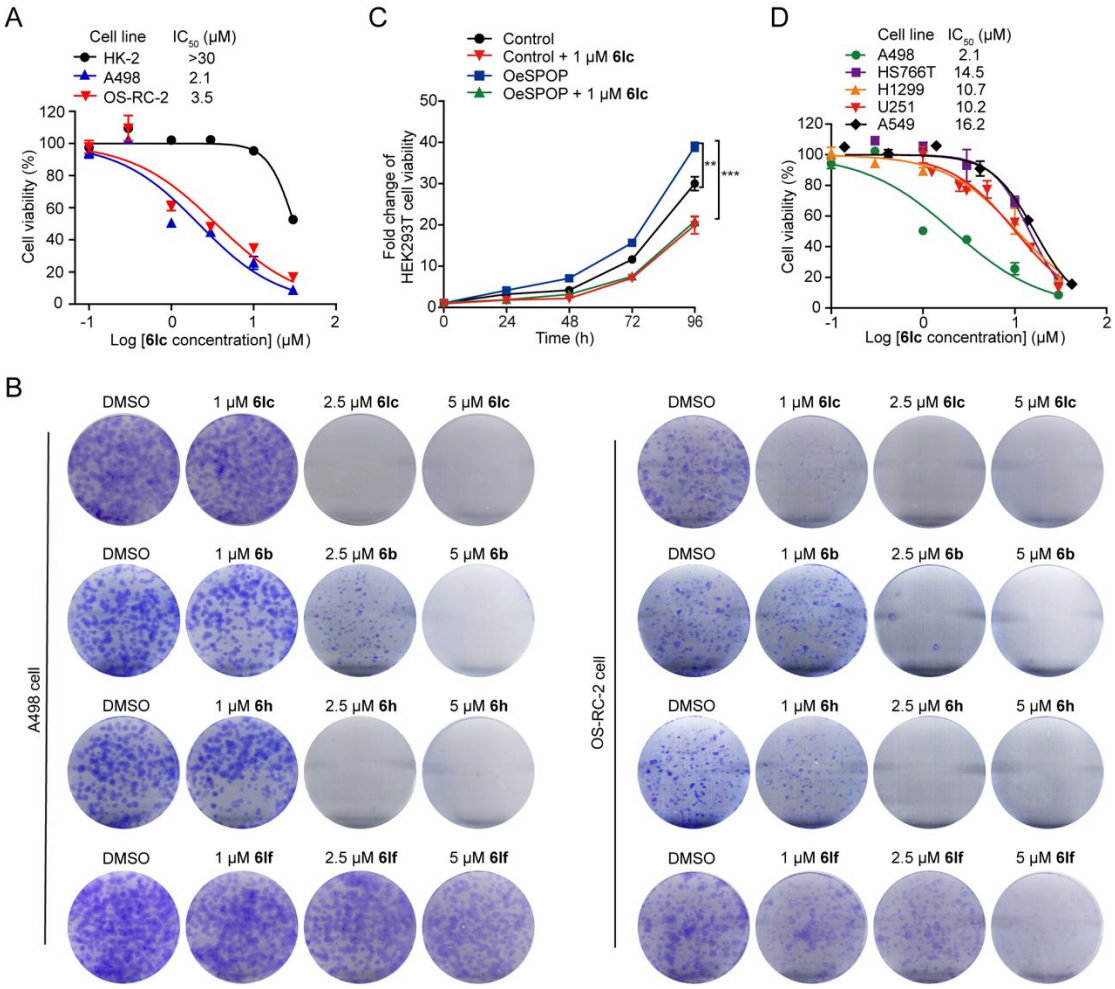

Figure 4. Antiproliferative effect of inhibitor **6lc**. (A) Quantitation of IC_{50} of **6lc** against the proliferation of ccRCC cell lines and HK-2 cells. (B) Effect of SPOP inhibitors on the colony formation of A498 and OS-RC-2 cell lines. (C) Effect of **6lc** on the proliferation in HEK293T cells overexpressing SPOP. (D) Effect of **6lc** on cell proliferation in other cancer cell lines. **, $p < 0.01$; ***, $p < 0.001$; unpaired Student's t-test. Error bar, mean ± SD, n = 3.

It has been previously shown that HEK293 cells do not express SPOP in the cytoplasm, but the overexpression of SPOP in HEK293T cells promotes tumorigenesis.[13] As expected, the recapitulated ccRCC phenotype observed in the

HEK293T cells of overexpressing SPOP could be suppressed by the treatment of the SPOP inhibitor **6lc** (Figure 4C), thus indicating compound **6lc** is specific to the inhibition of the cytoplasmic SPOP. Lastly, we also determined the effect of **6lc** on proliferation in other cancer cell lines in which SPOP is absent from the cytoplasm. By over five folds the IC_{50} for A498 cell proliferation measured less than that for four other tested cell lines (Figure 4D). Taken together, SPOP inhibitor **6lc** is likely specific to suppress the proliferation of cells driven by cytoplasmic SPOP rather than those cell lines in which SPOP is absent from the cytoplasm.

Characterizations of the interactions between SPOP and inhibitors *in vitro*. The Tm of $SPOP^{MATH}$ is shifted up to 3.5 ^{o}C in the presence of the 20-fold compound **6lc** (Table 1), suggesting that **6lc** binds to the substrate-binding MATH domain. We further performed the nanoDSF assay under native conditions on the $SPOP^{23-337}$ protein that contains both MATH and BTB domains. Compound **6lc** thermally stabilizes the $SPOP^{23-337}$ protein by elevating the Tm up to 2.1 ^{o}C even in an equal molar ratio (Figure 5A). Although the negative control compound **6c** exhibits little effect on the thermal stability of SPOP in nanoDSF measurement (Figure 5B), it appears that DMSO destabilizes SPOP and that the compound returns the Tm back to its usual state in the absence of DMSO. A similar phenomenon is observed in the conventional DSF screening, in which a fluorescent dye is required, although compound **6lc** significantly stabilizes $SPOP^{MATH}$ by shifting the Tm to 4 ^{o}C (Figure 5C). Again, the negative control **6c** had minimal effect on the stability of $SPOP^{MATH}$ in the conventional DSF assay (Figure 5D). Consistent with our previous conclusion that

SPOP inhibitor **6b** does not belong to the Pan Assay Interference Compound (PAINS),[14] neither the conventional DSF performed with mixtures of just the dye and compound **6lc** yields any changes in fluorescence, nor does the nanoDSF experiment conducted on compound **6lc** and unrelated proteins yield any changes in fluorescence, for example, the BSA and ClpP caused no changes in thermal stability. Instead of a fluorescence based DSF system, other biophysical methods, like Nuclear Magnetic Resonance (NMR) titration and Surface Plasmon Resonance (SPR) should also be better options in order to ensure that observed thermal effects are unlikely due to the conjugated nature or the large concentration of compound **6lc**. Attenuation of signals in Carr-Purcell-Meiboom-Gill (CPMG) NMR titrations alongside positive Saturation Transfer Difference (STD) signals are detected (Figures 5E and S2A), which indicates that both $SPOP^{MATH}$ and SPOP in full-length interfere with the state of compound **6lc**. In addition, SPR measurement has established a moderate affinity for inhibitor **6lc** binding to the two SPOP proteins, which is around 30 μM (Figure 5F and S2B). Lastly, a variety of SPOP inhibitors are observed to thermally stabilize SPOP in the conventional DSF assay (Figure 5G). Collectively, we performed different assays in order to confirm SPOP inhibitors binding to SPOP protein.

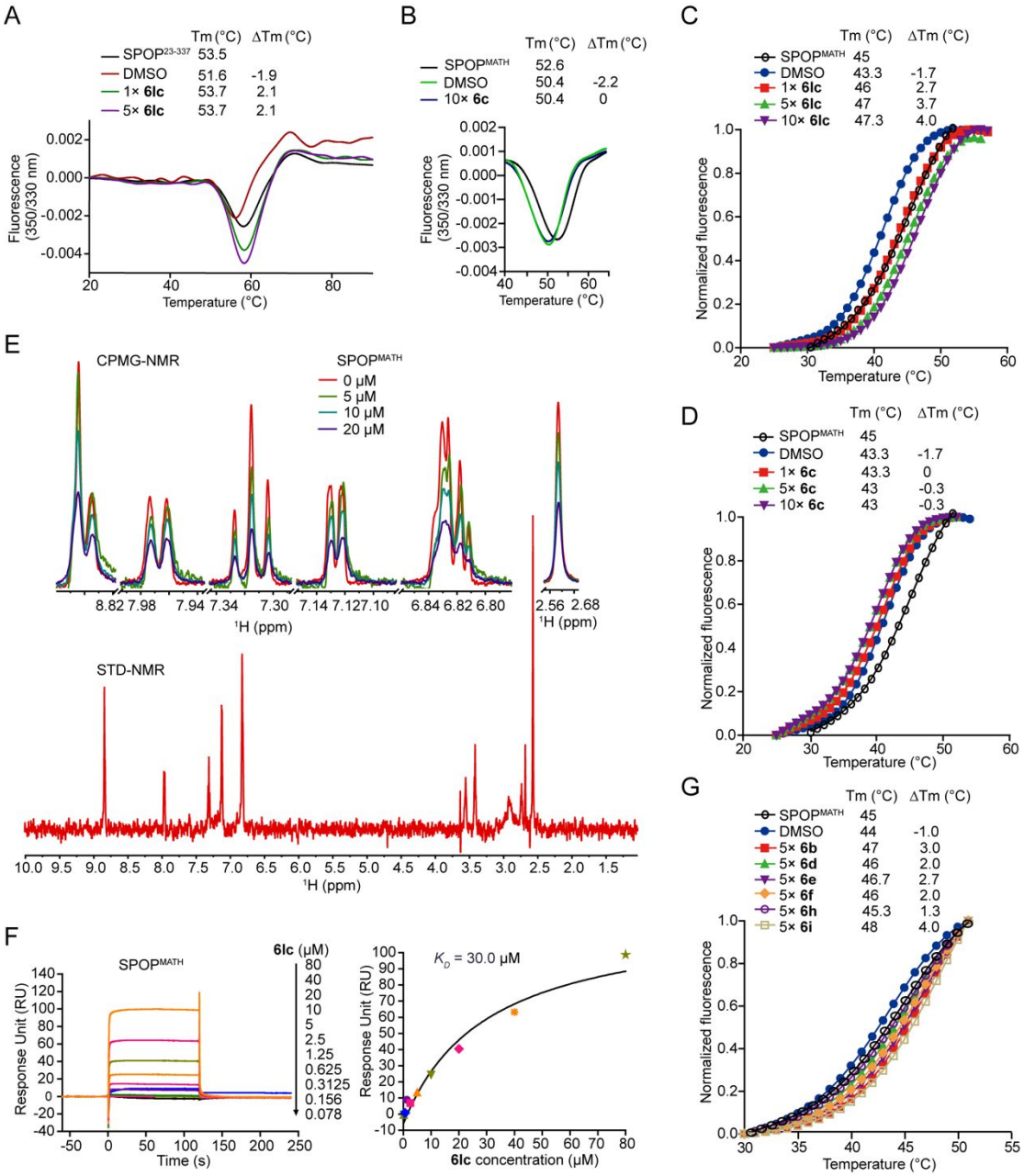

Figure 5. Investigations on the binding of inhibitors to SPOP *in vitro*. (A) Effect of **6lc** on the thermal stability of SPOP$^{23\text{-}337}$ in nanoDSF. (B) Effect of **6c** on the thermal stability of SPOP^{MATH} in nanoDSF. (C) Effect of **6lc** on the stability of SPOP^{MATH} in the conventional DSF assay. (D) Effect of **6c** on the stability of SPOP^{MATH} in the conventional DSF. (E) NMR measurement of **6lc** binding to SPOP^{MATH}. The STD-NMR spectrum for 200 μM **6lc** is recorded in the presence of SPOP^{MATH}. (F) Determination

of the affinity of **6lc** binding to $SPOP^{MATH}$ in SPR measurement. Graphs of equilibrium RU responses versus compound concentrations are plotted. (G) Effect of SPOP inhibitors on the stability of $SPOP^{MATH}$ in the conventional DSF assay. For nanoDSF and conventional DSF assay, ΔTm for DMSO-treated SPOP protein were calculated using a naive SPOP sample as the reference, while ΔTm data for the compound-treated SPOP were reported using DMSO-treated SPOP as the reference.

6lc inhibits SPOP-PTEN interaction. In order to verify the cellular interaction between **6lc** and SPOP, we performed a Drug Affinity Responsive Target Stability (DARTS) assay.[22] As expected, the SPOP protein becomes protease-resistant in the presence of **6lc** (Figure 6A), indicating the direct interaction of **6lc** with SPOP in cell lysates of both A498 and OS-RC-2 cells. Next, we performed the Co-immunoprecipitation (Co-IP) experiment in HEK293T cells in order to elucidate whether **6lc** could disrupt the SPOP-mediated protein interaction. As shown in Figure 6B, the SPOP-binder **6lc** is able to inhibit SPOP-binding with its substrate-protein PTEN in a dose-dependent manner. Consequently, the abundance of ubiquitinated PTEN protein is steadily reduced when HEK293T cells are exposed to the compound **6lc** in a concentration-dependent way (Figures 6C).

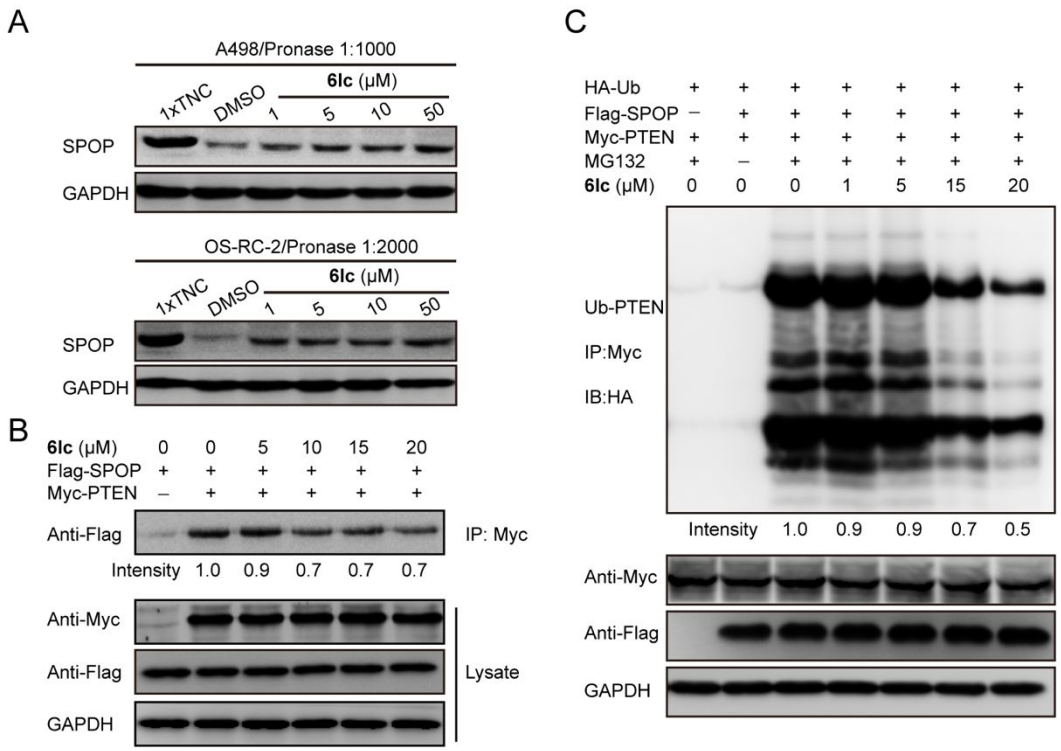

Figure 6. Effect of **6lc** on the interaction with SPOP and the disruption of the SPOP-PTEN interaction in HEK293T cells. (A) Representative western blots for SPOP levels in A498 and OS-RC-2 cells in DARTS. (B) Effect of **6lc** on SPOP interaction with PTEN in intact HEK293T cells in Co-IP assay. (C) Effect of **6lc** on ubiquitination of PTEN in HEK193T cells. The intensity in the western blot was read with ImageJ. All experiments were performed in triplicate.

6lc disrupts the oncogenic SPOP-signaling pathway in kidney cancer cells. Both PTEN and DUSP7 are tumor suppressors that regulate cell proliferation and apoptosis through the cytoplasmic SPOP-signaling pathway in ccRCC.[13] We have previously demonstrated that SPOP inhibitors biochemically illuminate in cells the therapeutic potential of blocking SPOP activity to stabilize PTEN and DUSP7, which suppresses the AKT- and ERK-driven cancer-signaling pathways. Indeed, a steady

accumulation of PTEN and DUSP7 proteins is observed in a dose-dependent manner when A498 and OS-RC-2 cell lines are exposed to compound **6lc** for 12 hr (Figure 7A). Therefore, the accumulation of PTEN and DUSP7 in the cytoplasm subsequently results in decreases of phosphorylated AKT and ERK in both ccRCC cell lines. The total cellular abundance of AKT and ERK proteins in A498 and OS-RC-2 cells remains constant in the presence of compound **6lc**. Of note, Real-time quantitative PCR (RT-qPCR) experiments showed that changes of PTEN and DUSP6 in A498 and OS-RC-2 ccRCC cell lines are not at the transcription level (Figure 7B). In addition, several analogs of **6lc**, namely compound **6lf**, **6li**, **6i**, and **6l**, also lead to the stabilization and accumulation of PTEN protein in OS-RC-2 cells (Figure 7C).

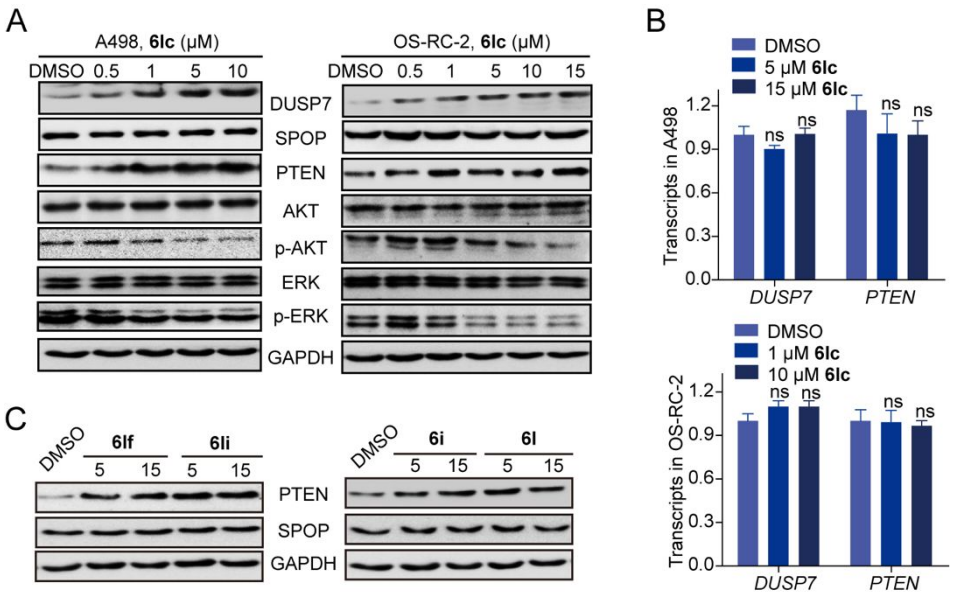

Figure 7. Effect of SPOP inhibitor on the oncogenic SPOP-signaling pathway in kidney cancer cells. (A) Effect of **6lc** on the protein levels in the SPOP-signaling pathway in A498 and OS-RC-2 cell lines. (B) Effect of **6lc** on the transcription of *PTEN* and *DUSP7*

in A498 and OS-RC-2 cell lines. (C) Effect of SPOP inhibitors on the PTEN level in OS-RC-2 cells. All experiments were performed in triplicate.

CONCLUSION

We performed synthetic optimization based on the previously established chemical scaffold to explore the SAR for potent SPOP inhibitors. We tested five sets of **6b** analogs to better understand which motifs in the molecule are important for SPOP engagement. A nanoDSF-based high-throughput assay, that measures the thermal stability of an interested protein, is applied as an initial screening of small-molecule binders for SPOP protein. Then, the antiproliferative activities against A498 and OS-RC-2 cell lines are evaluated, and the SAR is elucidated. Most amide analogs thermally stabilize SPOP protein and exhibit antiproliferations in ccRCC cells, which suggests that the nanoDSF is an option for the initial screening of SPOP inhibitors. Compound **6lc** exhibits strong inhibitory potency against both ccRCC cell lines with IC_{50} of 2.1 μM and 3.5 μM, respectively. Additionally, compound **6lc** significantly inhibits the colony formation for both A498 and OS-RC-2 cell lines, superior to our previously reported **6b** and other analogs tested. The performance of different assays, including DSF, NMR titration, SPR analysis, and DARTS assay has confirmed that inhibitor **6lc** directly interacts with the SPOP protein *in vitro* and in cell lysates. Lastly, an in-depth mechanistic study has revealed that compound **6lc** disrupts SPOP-substrate protein interaction in both ccRCC cell lines, and as a consequence leads to the stabilization and accumulation of tumor suppressors PTEN and DUSP7 and reduced abundances of phosphorylated AKT and ERK in the downstream. Taken

together, we have demonstrated that the SPOP inhibitor **6lc** represents a new lead for further improvement to sufficiently target the cytoplasmic SPOP-signaling pathway in ccRCC, which stands as a promising strategy to combat kidney cancer. Although SPOP has also been shown to be a tumor suppressor in prostate cancer, it is important to note that inhibition of SPOP may not be a strategy for all cancers.

EXPERIMENTAL SECTION

Chemistry. Unless otherwise stated, all solvents and reagents were purchased from commercial sources and used as received. ^{1}HNMR and ^{13}CNMR spectra were recorded with a Varian-MERCURY Plus-400, 500, and 600 NMR spectrometer at rt. NMR spectra were calibrated to the solvent signals of DMSO-d_6, TFA-*d*, MeOD, or $CDCl_3$. Chemical shifts are reported in ppm (δ scale) as referenced to TMS and coupling constant (*J*) values are reported in hertz (Hz). Data are presented as follows: chemical shift, multiplicity (s = singlet, d = doublet, dd = doublet of doublet, t = triplet, q = quartet, m = multiplet, br = broad), *J* in Hz, and integration. Flash-column chromatography was performed using silica gel (230–400 mesh). Analytical TLC was performed on silica gel plates and visualized under ultraviolet light (254 nm). The purity and LRMS of all the synthesized compounds were determined by LCMS (Agilent 1200LC/G6110A, XBridge, 4.6 × 50 mm, 3.5 µm, 50 °C, flow rate = 1.8 mL/min) with aqueous CH_3CN and water (10 mM Ammonium hydrogen carbonate or 0.01% TFA). The purities of all target compounds are >95% in HPLC.

Synthetic procedure for compound 2. A mixture of 3-methylpyridin-2-amine **1** and diethyl malonate was stirred at 220 °C for 2 hr. The generated ethanol was distilled during reaction. The residue was recrystallized from ethanol to give product **2**.

Synthetic procedure for compound 3. To a cool DMF (144 mL) $POCl_3$ (44 g, 288 mmol, 4.0 eq) was added dropwise. After the mixture was stirred for 30 min at 0 °C, compound **2** (11.8 g, 72 mmol) was added slowly. The reaction was continued at 0 °C for 1 hr and at rt for 1 hr, and then was refluxed for another 1 hr. The mixture was poured into ice water and stirred for 1 hr. The precipitate was filtered and washed thoroughly with cold water. After a period of vacuum drying, compound **3** (10.2 g, 63.8% yield) was collected. ^{1}H NMR (400 MHz, DMSO-d_6) δ 10.25 (s, 1H), 9.08 – 8.99 (m, 1H), 8.25 (d, *J* = 6.8 Hz, 1H), 7.58 (t, *J* = 7.0 Hz, 1H), 2.53 (s, 3H).

Synthetic procedure for compound 4. A mixture of intermediate **3** (446 mg, 2 mmol, 1.0 eq) and corresponding amine (8 mmol, 4.0 eq) in EtOH (4 mL) was stirred at rt overnight in the presence of anhydrous Na_2SO_4 (100 mg). The precipitate was filtered and washed with EtOH. The solid was re-dissolved in CH_2Cl_2 and filtered in order to remove Na_2SO_4. Compound **4** was obtained after the evaporation of the solvent under reduced pressure in good yields. Compounds **4k** and **4p** were directly used in the next step without purification or NMR data collection.

(E)-9-methyl-2-((4-methylphenethyl)amino)-3-(((4-methylphenethyl)imino)methyl)-4H-pyrido[1,2-a]pyrimidin-4-one (4d). White solid (400 mg, 46% yield). ^{1}H NMR (400 MHz, $CDCl_3$) δ 10.73 (s, 1H), 8.88 (s, 1H), 8.81 (d, *J*

= 6.4 Hz, 1H), 7.49 (d, *J* = 6.7 Hz, 1H), 7.18 (dd, *J* = 8.2, 2.3 Hz, 4H), 7.14 (d, *J* = 6.0 Hz, 4H), 6.79 (t, *J* = 7.0 Hz, 1H), 3.88 – 3.72 (m, 4H), 2.94 – 2.87 (m, 2H), 2.85 (dd, *J* = 15.5, 8.1 Hz, 2H), 2.49 (s, 3H), 2.35 (s, 3H), 2.34 (s, 3H).

(E)-2-((4-methoxyphenethyl)amino)-3-(((4-methoxyphenethyl)imino)methyl)-9-methyl-4H-pyrido[1,2-a]pyrimidin-4-one (4e). White solid (452 mg, 48% yield). ^{1}H NMR (400 MHz, $CDCl_3$) δ 10.72 (s, 0H), 8.87 (s, 0H), 8.80 (d, *J* = 6.9 Hz, 0H), 7.48 (d, *J* = 6.7 Hz, 0H), 7.20 (d, *J* = 8.6 Hz, 1H), 7.15 (d, *J* = 8.6 Hz, 1H), 6.93 – 6.84 (m, 1H), 6.77 (t, *J* = 7.0 Hz, 0H), 3.91 – 3.73 (m, 10H), 2.88 (t, *J* = 7.4 Hz, 2H), 2.84 (dd, *J* = 14.7, 7.4 Hz, 2H), 2.48 (s, 3H).

(E)-2-((4-fluorophenethyl)amino)-3-(((4-fluorophenethyl)imino)methyl)-9-methyl-4H-pyrido[1,2-a]pyrimidin-4-one (4f). White solid (473 mg, 53% yield). ^{1}H NMR (500 MHz, $CDCl_3$) δ 10.61 (s, 1H), 8.83 (s, 1H), 8.78 (d, *J* = 6.7 Hz, 1H), 7.47 (d, *J* = 6.1 Hz, 1H), 7.24 – 7.11 (m, 4H), 6.98 (dt, *J* = 12.8, 8.5 Hz, 4H), 6.77 (t, *J* = 6.7 Hz, 1H), 3.86 – 3.67 (m, 4H), 2.87 (t, *J* = 6.9 Hz, 2H), 2.82 (t, *J* = 6.7 Hz, 2H), 2.46 (s, 3H).

(E)-2-((4-chlorophenethyl)amino)-3-(((4-chlorophenethyl)imino)methyl)-9-methyl-4H-pyrido[1,2-a]pyrimidin-4-one (4g). White solid (556 mg, 58% yield). ^{1}H NMR (400 MHz, $CDCl_3$) δ 10.60 (s, 1H), 8.85 (s, 1H), 8.81 (d, *J* = 6.7 Hz, 1H), 7.50 (d, *J* = 6.7 Hz, 1H), 7.28 (ddd, *J* = 10.8, 5.7, 2.1 Hz, 5H), 7.15 (dd, *J* = 15.3, 8.3 Hz, 4H), 6.80 (t, *J* = 7.0 Hz, 1H), 3.87 – 3.71 (m, 4H), 2.88 (t, *J* = 7.2 Hz, 2H), 2.83 (t, *J* = 7.1 Hz, 2H), 2.48 (s, 3H).

(E)-2-((4-bromophenethyl)amino)-3-(((4-bromophenethyl)imino)methyl)-9-methyl-4H-pyrido[1,2-a]pyrimidin-4-one (4h). White solid (466 mg, 41% yield).^{1}H NMR (400 MHz, $CDCl_3$) δ 10.58 (s, 1H), 8.85 (s, 1H), 8.80 (d, *J* = 7.0 Hz, 1H), 7.50 (d, *J* = 6.7 Hz, 1H), 7.43 (dd, *J* = 12.1, 5.4 Hz, 4H), 7.10 (dd, *J* = 13.5, 8.3 Hz, 4H), 6.79 (t, *J* = 7.0 Hz, 1H), 3.78 (dt, *J* = 14.4, 7.1 Hz, 4H), 2.86 (t, *J* = 7.2 Hz, 2H), 2.81 (t, *J* = 7.0 Hz, 2H), 2.47 (s, 3H).

(E)-2-((3-fluorophenethyl)amino)-3-(((3-fluorophenethyl)imino)methyl)-9-methyl-4H-quinolizin-4-one (4i). White solid (339 mg, 38% yield). ^{1}H NMR (600 MHz, CDCl3) δ 10.62 (s, 1H), 8.84 (s, 1H), 8.79 (d, *J* = 7.0 Hz, 1H), 7.48 (d, *J* = 6.6 Hz, 1H), 7.28 – 7.20 (m, 2H), 7.01 (d, *J* = 7.5 Hz, 1H), 6.99 – 6.94 (m, 2H), 6.94 – 6.87 (m, 3H), 6.78 (t, *J* = 6.9 Hz, 1H), 3.80 (m, 4H), 2.90 (t, *J* = 7.3 Hz, 2H), 2.85 (t, *J* = 7.0 Hz, 2H), 2.47 (s, 3H).

(E)-2-((2-fluorophenethyl)amino)-3-(((2-fluorophenethyl)imino)methyl)-9-methyl-4H-pyrido[1,2-a]pyrimidin-4-one (4j). White solid (552 mg, 62% yield). ^{1}H NMR (400 MHz, $CDCl_3$) δ 10.47 (s, 1H), 8.66 (d, *J* = 1.0 Hz, 1H), 8.58 (d, *J* = 7.0 Hz, 1H), 7.27 (d, *J* = 6.7 Hz, 1H), 7.08 – 6.94 (m, 4H), 6.95 – 6.79 (m, 4H), 6.56 (t, *J* = 6.9 Hz, 1H), 3.73 – 3.52 (m, 4H), 2.76 (dt, *J* = 19.0, 7.1 Hz, 4H), 2.27 (s, 3H).

(E)-9-methyl-2-((2-(thiophen-2-yl)ethyl)amino)-3-(((2-(thiophen-2-yl)ethyl)imino)methyl)-4H-pyrido[1,2-a]pyrimidin-4-one (4l). Yellow solid (532 mg, 63% yield). ^{1}H NMR (400 MHz, $CDCl_3$) δ 10.61 (s, 1H), 8.70 (s, 1H), 8.61 (d, *J* = 6.9 Hz, 1H), 7.30 (d, *J* = 6.0 Hz, 1H), 6.98 (dd, *J* = 11.7, 5.1 Hz, 1H), 6.84 – 6.74 (m, 1H), 6.71

(s, 0H), 6.65 (s, 0H), 6.60 (t, *J* = 6.9 Hz, 0H), 3.89 – 3.52 (m, 4H), 2.97 (dt, *J* = 28.4, 6.9 Hz, 4H), 2.29 (s, 3H).

(E)-9-methyl-2,3-bis((2-morpholinoethyl)amino)-4H-pyrido[1,2-a]pyrimidin-4-one (4m). Yellow solid (483 mg, 58% yield). ^{1}H NMR (400 MHz, $CDCl_3$) δ 10.69 (s, 1H), 8.91 (s, 1H), 8.80 (d, *J* = 7.1 Hz, 1H), 7.49 (d, *J* = 6.8 Hz, 1H), 6.79 (t, *J* = 7.0 Hz, 1H), 3.82 – 3.71 (m, 12H), 2.74 – 2.63 (m, 4H), 2.56 (d, J = 3.8 Hz, 8H), 2.45 (s, 3H).

(E)-9-methyl-2-((3-phenylpropyl)amino)-3-(((3-phenylpropyl)imino)methyl)-4H-pyrido[1,2-a]pyrimidin-4-one (4n). Yellow solid (483 mg, 58% yield). ^{1}H NMR (400 MHz, $CDCl_3$) δ 10.65 (s, 1H), 8.74 (s, 1H), 8.60 (d, *J* = 7.1 Hz, 1H), 7.25 (d, *J* = 6.6 Hz, 1H), 7.22 – 6.88 (m, 11H), 6.56 (t, *J* = 6.9 Hz, 1H), 3.71 – 3.37 (m, 4H), 2.55 (dd, *J* = 17.2, 9.0 Hz, 5H), 2.20 (s, 4H), 2.01 – 1.74 (m, 4H).

(E)-9-methyl-2-((2-phenoxyethyl)amino)-3-(((2-phenoxyethyl)imino)methyl)-4H-pyrido[1,2-a]pyrimidin-4-one (4o). White solid (465 mg, 53% yield). ^{1}H NMR (600 MHz, $CDCl_3$) δ 10.91 (s, 1H), 8.97 (s, 1H), 8.80 (d, *J* = 6.8 Hz, 1H), 7.48 (d, *J* = 6.4 Hz, 1H), 7.27 – 7.22 (m, 4H), 6.91 (ddd, *J* = 23.7, 15.7, 7.8 Hz, 6H), 6.78 (t, *J* = 6.9 Hz, 1H), 4.18 (dd, *J* = 11.3, 5.9 Hz, 4H), 4.02 (dd, *J* = 10.3, 5.0 Hz, 2H), 3.95 (s, 2H), 2.43 (s, 3H).

(E)-2-(benzylamino)-3-((benzylimino)methyl)-9-methyl-4H-pyrido[1,2-a]pyrimidin-4-one (4q). Yellow solid (574 mg, 75% yield). ^{1}H NMR (400 MHz, $CDCl_3$) δ 11.20 (s, 1H), 9.08 (s, 1H), 8.89 – 8.82 (m, 1H), 7.47 (d, *J* = 6.7 Hz, 1H), 7.41 – 7.23 (m, 10H), 6.79 (t, *J* = 7.0 Hz, 1H), 4.86 (d, *J* = 5.7 Hz, 2H), 4.80 (s, 2H), 2.44 (s, 3H).

(E)-9-methyl-2,3-bis((pyridin-4-ylmethyl)amino)-4H-pyrido[1,2-a]pyrimidin-4-one (4r). Yellow solid (358 mg, 48% yield). ^{1}H NMR (400 MHz, $CDCl_3$) δ 11.03 (t, *J* = 5.7 Hz, 1H), 9.08 (s, 1H), 8.83 (d, *J* = 7.2 Hz, 1H), 8.56 – 8.52 (m, 4H), 7.52 (dd, *J* = 6.8, 1.1 Hz, 1H), 7.25 (d, *J* = 6.0 Hz, 2H), 7.22 (d, *J* = 6.0 Hz, 2H), 6.86 (t, *J* = 7.0 Hz, 1H), 4.86 (d, *J* = 5.9 Hz, 2H), 4.80 (s, 2H), 2.35 (s, 3H).

(E)-9-methyl-2-(phenylamino)-3-((phenylimino)methyl)-4H-pyrido[1,2-a]pyrimidin-4-one (4s). Yellow solid (610 mg, 86% yield). ^{1}H NMR (600 MHz, $CDCl_3$) δ 13.22 (s, 1H), 9.20 (s, 1H), 8.82 (dd, *J* = 7.0, 0.6 Hz, 1H), 7.84 (d, *J* = 7.6 Hz, 2H), 7.50 (d, *J* = 6.7 Hz, 1H), 7.41 (dd, *J* = 11.0, 4.6 Hz, 2H), 7.33 (ddd, *J* = 9.3, 8.2, 4.2 Hz, 4H), 7.23 (dd, *J* = 13.9, 6.6 Hz, 1H), 7.09 (t, *J* = 7.4 Hz, 1H), 6.82 (t, *J* = 6.9 Hz, 1H), 2.48 (s, 3H).

(E)-2-(cyclohexylamino)-3-((cyclohexylimino)methyl)-9-methyl-4H-pyrido[1,2-a]pyrimidin-4-one (4t). Yellow solid (506 mg, 69% yield). ^{1}H NMR (600 MHz, $CDCl_3$) δ 11.01 (d, *J* = 6.5 Hz, 1H), 8.91 (s, 1H), 8.77 (d, *J* = 7.0 Hz, 1H), 7.42 (d, *J* = 6.6 Hz, 1H), 6.71 (t, *J* = 6.9 Hz, 1H), 4.29 – 4.15 (m, 1H), 3.21 (dd, *J* = 10.9, 7.7 Hz, 1H), 2.41 (s, 3H), 2.00 (d, *J* = 7.5 Hz, 2H), 1.87 – 1.72 (m, 6H), 1.69 – 1.57 (m, 2H), 1.53 – 1.37 (m, 9H).

(E)-9-methyl-2,3-bis(methylamino)-4H-pyrido[1,2-a]pyrimidin-4-one (4u). White solid (249 mg, 57% yield). ^{1}H NMR (400 MHz, $CDCl_3$) δ 10.41 (s, 1H), 8.89 (d, *J* = 1.1 Hz, 1H), 8.80 (d, *J* = 7.2 Hz, 1H), 7.47 (d, *J* = 6.8 Hz, 1H), 6.77 (t, *J* = 7.0 Hz, 1H), 3.46 (d, *J* = 0.9 Hz, 3H), 3.13 (d, *J* = 3.7 Hz, 3H), 2.45 (s, 3H).

(E)-2-(isopropylamino)-3-((isopropylimino)methyl)-9-methyl-4H-pyrido[1,2-a]pyrimidin-4-one (4v). White solid (281 mg, 49% yield). ^{1}H NMR (400 MHz, $CDCl_3$) δ

10.88 (d, *J* = 5.7 Hz, 1H), 8.91 (s, 1H), 8.79 (d, *J* = 7.1 Hz, 1H), 7.45 (d, *J* = 6.7 Hz, 1H), 6.74 (t, *J* = 7.0 Hz, 1H), 4.44 (dp, *J* = 13.2, 6.5 Hz, 1H), 3.51 (dt, *J* = 12.5, 6.3 Hz, 1H), 2.44 (s, 3H), 1.33 (d, *J* = 6.5 Hz, 6H), 1.24 (d, *J* = 6.3 Hz, 6H).

(E)-9-methyl-2,3-bis(propylamino)-4H-pyrido[1,2-a]pyrimidin-4-one (4w). Yellow solid (236 mg, 43% yield). ^{1}H NMR (400 MHz, $CDCl_3$) δ 10.80 (s, 1H), 8.90 (s, 1H), 8.80 (d, *J* = 7.0 Hz, 1H), 7.47 (d, *J* = 6.6 Hz, 1H), 6.77 (t, *J* = 6.9 Hz, 1H), 3.68 – 3.51 (m, 4H), 2.45 (s, 3H), 1.79 – 1.63 (m, 5H), 1.01 (dt, *J* = 17.6, 7.4 Hz, 7H).

(E)-9-methyl-2,3-bis(prop-2-yn-1-ylamino)-4H-pyrido[1,2-a]pyrimidin-4-one (4x). Yellow solid (261 mg, 49% yield). ^{1}H NMR (400 MHz, $CDCl_3$) δ 10.56 (s, 1H), 9.13 (t, *J* = 1.4 Hz, 1H), 8.82 (d, *J* = 7.1 Hz, 1H), 7.54 (d, *J* = 6.8 Hz, 1H), 6.85 (t, *J* = 7.0 Hz, 1H), 4.55 – 4.32 (m, 4H), 2.49 (s, 4H), 2.24 (t, *J* = 2.5 Hz, 1H).

(E)-2-((2-(1H-indol-3-yl)ethyl)amino)-3-(((2-(1H-indol-3-yl)ethyl)imino)methyl)-9-methyl-4H-pyrido[1,2-a]pyrimidin-4-one (4y). Yellow solid (616 mg, 63% yield). ^{1}H NMR (400 MHz, $CDCl_3$) δ 10.77 (s, 1H), 8.94 (s, 1H), 8.81 (d, *J* = 7.0 Hz, 1H), 7.89 (s, 1H), 7.68 (d, *J* = 7.6 Hz, 2H), 7.63 (d, *J* = 7.7 Hz, 1H), 7.47 (d, *J* = 6.4 Hz, 1H), 7.41 – 7.09 (m, 8H), 6.90 (s, 1H), 6.75 (dd, *J* = 14.6, 7.6 Hz, 2H), 3.91 (dd, *J* = 12.3, 6.3 Hz, 2H), 3.85 (t, *J* = 6.6 Hz, 2H), 3.09 (t, *J* = 6.6 Hz, 2H), 2.98 (t, *J* = 6.7 Hz, 2H), 2.48 (s, 3H).

(E)-2-((4-chlorophenyl)amino)-3-(((4-chlorophenyl)imino)methyl)-9-methyl-4H-pyrido[1,2-a]pyrimidin-4-one (4z). Yellow solid (660 mg, 78% yield). ^{1}H NMR (600 MHz, $CDCl_3$) δ 13.09 (s, 1H), 9.16 (s, 1H), 8.85 (dd, *J* = 7.0, 0.7 Hz, 1H), 7.80 – 7.75 (m,

2H), 7.60 (d, *J* = 6.7 Hz, 1H), 7.38 – 7.34 (m, 2H), 7.33 – 7.29 (m, 2H), 7.25 – 7.20 (m, 2H), 6.91 (t, *J* = 6.9 Hz, 1H), 2.50 (s, 3H).

Synthetic procedure for α-cyanoacetamide 5. The mixture of ethyl 2-cyanoacetate (1243 mg, 11 mmol, 1.1 eq) and corresponding amine (10 mmol, 1.0 eq) was stirred at rt. After the consumption of amine monitored by TLC, the precipitate was filtered and washed thoroughly with ether. Then, the intermediate α-cyanoacetamide **5** was obtained in high yields.

2-cyano-N-(3-morpholinopropyl)acetamide (5a). Brown solid (1.86 g, 88% yield). ^{1}H NMR (400 MHz, $CDCl_3$) δ 7.90 (s, 1H), 3.82 – 3.76 (m, 4H), 3.43 (dd, *J* = 11.6, 5.7 Hz, 2H), 2.57 – 2.43 (m, 6H), 1.80 – 1.66 (m, 2H).

2-cyano-N-(3-phenylpropyl)acetamide (5b). White solid (1.56 g, 77% yield). ^{1}H NMR (400 MHz, MeOD) δ 7.28 (t, *J* = 7.4 Hz, 2H), 7.24 – 7.14 (m, 3H), 4.91 (s, 3H), 3.23 (t, *J* = 7.0 Hz, 2H), 2.66 (t, *J* = 7.7 Hz, 2H), 1.91 – 1.78 (m, 2H).

2-cyano-N-(2-morpholinoethyl)acetamide (5c). White solid (1.49 g, 76% yield). ^{1}H NMR (400 MHz, MeOD) δ 4.92 (s, 2H), 3.79 – 3.66 (m, 2H), 3.39 (t, *J* = 6.5 Hz, 1H), 3.33 (s, 1H), 2.52 (t, *J* = 6.4 Hz, 3H).

2-cyano-N-(2-(4-methylpiperazin-1-yl)ethyl)acetamide (5d). White solid (1.80 g, 86% yield). ^{1}H NMR (400 MHz, MeOD) δ 4.92 (s, 3H), 3.38 (t, *J* = 6.6 Hz, 2H), 2.53 (t, *J* = 6.6 Hz, 8H), 2.31 (s, 3H).

2-cyano-N-phenethylacetamide (5e). White solid (1.43 g, 76% yield). ^{1}H NMR (400 MHz, $CDCl_3$) δ 7.34 (m, 2H), 7.30 – 7.24 (m, 1H), 7.22 (d, *J* = 7.1 Hz, 2H), 6.48 (s, 1H), 3.62 – 3.50 (m, 2H), 3.31 (s, 2H), 2.86 (t, *J* = 7.0 Hz, 2H).

2-cyano-N-(4-fluorophenethyl)acetamide (5f). White solid (1.63 g, 79% yield). ^{1}H NMR (400 MHz, $CDCl_3$) δ 7.20 – 7.11 (m, 2H), 7.00 (t, *J* = 8.5 Hz, 2H), 6.60 (s, 1H), 3.51 (q, *J* = 6.7 Hz, 2H), 3.35 (s, 2H), 2.82 (t, *J* = 7.1 Hz, 2H).

2-cyano-N-(4-methoxyphenethyl)acetamide (5g). White solid (1.58 g, 72% yield). ^{1}H NMR (400 MHz, MeOD) δ 7.14 (d, *J* = 8.6 Hz, 1H), 6.86 (d, *J* = 8.6 Hz, 1H), 4.92 (s, 2H), 3.77 (s, 3H), 3.41 (t, *J* = 7.3 Hz, 2H), 2.76 (t, *J* = 7.3 Hz, 2H).

N-benzyl-2-cyanoacetamide (5h). White solid (1.36 g, 78% yield). ^{1}H NMR (400 MHz, $CDCl_3$) δ 7.45 – 7.23 (m, 5H), 6.72 (m, 1H), 4.43 (s, 2H), 3.35 (s, 2H).

2-cyano-N-((tetrahydrofuran-2-yl)methyl)acetamide (5i). White solid (1.27 g, 76% yield). ^{1}H NMR (400 MHz, MeOD) δ 4.91 (s, 3H), 3.99 (s, 1H), 3.88 (s, 1H), 3.76 (s, 1H), 3.31 (d, *J* = 15.8 Hz, 3H), 1.94 (s, 3H), 1.60 (s, 1H).

2-cyano-N-cyclohexylacetamide (5j). White solid (1.18 g, 71% yield). ^{1}H NMR (400 MHz, $CDCl_3$) δ 6.19 (s, 1H), 3.85 – 3.67 (m, 1H), 3.38 (s, 2H), 1.93 (d, *J* = 12.0 Hz, 2H), 1.74 (d, *J* = 13.3 Hz, 2H), 1.64 (d, *J* = 13.0 Hz, 1H), 1.37 (dd, *J* = 24.7, 12.5 Hz, 2H), 1.31 – 1.10 (m, 3H).

2-cyano-N-(2-hydroxyethyl)acetamide (5k). White solid (937 mg, 73% yield). ^{1}H NMR (400 MHz, MeOD) δ 4.90 (s, 2H), 3.63 (t, *J* = 5.6 Hz, 2H), 3.34 (t, *J* = 5.6 Hz, 2H).

General synthetic procedure for compound 6. A mixture containing α-cyanoacetamide **5** (0.3 mmol, 1.5 eq) and corresponding imine intermediate **4** (0.2 mmol, 1.0 eq) in $CHCl_3$ was refluxed overnight in the presence of a catalytic amount of piperidine. The yellow mixture was concentrated in vacuum. Product **6** was obtained by recrystallization from EtOH in high yields.

2-imino-10-methyl-1-(4-methylphenethyl)-N-(3-morpholinopropyl)-5-oxo-1,5-dihydro-2H-dipyrido[1,2-a:2',3'-d]pyrimidine-3-carboxamide (6d). Yellow solid (72 mg, 69% yield). ^{1}H NMR (400 MHz, $CDCl_3$) δ 8.90 (d, *J* = 6.2 Hz, 1H), 7.66 (d, *J* = 6.7 Hz, 1H), 7.23 (d, *J* = 7.5 Hz, 2H), 7.15 (d, *J* = 7.7 Hz, 2H), 7.02 (t, *J* = 7.0 Hz, 1H), 4.58 (s, 2H), 3.72 (t, *J* = 4.6 Hz, 4H), 3.53 (dd, *J* = 12.0, 6.4 Hz, 2H), 3.01 (t, *J* = 8.1 Hz, 2H), 2.61 (s, 3H), 2.49 (s, 6H), 2.33 (s, 3H), 1.89 – 1.76 (m, 2H). ^{13}C NMR (151 MHz, $CDCl_3$) δ 156.1, 150.1, 136.9, 133.9, 129.3, 128.5, 126.1, 114.1, 66.9, 53.7, 43.5, 32.3, 21.0, 18.1. LRMS m/z 515.2 $[M + H]^+$. HPLC purity 97.6%, t_r = 2.04 min.

2-imino-1-(4-methoxyphenethyl)-10-methyl-N-(3-morpholinopropyl)-5-oxo-1,5-dihydro-2H-dipyrido[1,2-a:2',3'-d]pyrimidine-3-carboxamide (6e). Yellow solid (75 mg, 71% yield). ^{1}H NMR (400 MHz, $CDCl_3$) δ 8.92 (d, *J* = 6.7 Hz, 1H), 8.66 (s, 1H), 7.69 (d, *J* = 6.8 Hz, 1H), 7.26 (s, 1H), 7.05 (t, *J* = 7.0 Hz, 1H), 6.89 (d, *J* = 8.6 Hz, 1H), 4.63 (s, 1H), 3.81 (s, 2H), 3.75 (t, *J* = 4.6 Hz, 4H), 3.55 (dd, *J* = 11.6, 6.3 Hz, 2H), 3.03 (d, *J* = 8.1 Hz, 2H), 2.63 (s, 3H), 2.59 – 2.47 (m, 6H), 1.89 – 1.80 (m, 3H). ^{13}C NMR (151 MHz, $CDCl_3$) δ 158.3, 156.1, 155.4, 152.8, 150.1, 136.9, 133.9, 129.7, 126.1, 114.1, 66.9, 55.2, 53.7, 43.7, 31.8, 18.1. LRMS m/z 531.2 $[M + H]^+$. HPLC purity 96.6%, t_r = 1.93 min.

1-(4-fluorophenethyl)-2-imino-10-methyl-N-(3-morpholinopropyl)-5-oxo-1,5-dihydro-2H-dipyrido[1,2-a:2',3'-d]pyrimidine-3-carboxamide (6f). Yellow solid (77 mg, 74% yield). ^{1}H NMR (400 MHz, $CDCl_3$) δ 8.88 (d, *J* = 6.9 Hz, 1H), 7.67 (d, *J* = 6.7 Hz, 1H), 7.29 (t, *J* = 6.3 Hz, 2H), 7.02 (dd, *J* = 16.0, 7.9 Hz, 3H), 4.62 (s, 1H), 3.73 (t, *J* = 4.4 Hz, 6H), 3.54 (dd, *J* = 11.6, 6.0 Hz, 2H), 3.04 (t, *J* = 7.9 Hz, 2H), 2.59 (s, 3H), 2.51 (s, 3H), 1.82 (m, *J* = 6.4 Hz, 2H). ^{13}C NMR (151 MHz, $CDCl_3$) δ 162.5, 160.9, 156.1, 150.2, 137.1, 133.9, 130.3, 126.2, 115.5, 114.3, 67.0, 53.8, 43.4, 32.0, 18.2. LRMS m/z 519.2 $[M + H]^+$. HPLC purity 97.2%, t_r = 1.96 min.

1-(4-chlorophenethyl)-2-imino-10-methyl-N-(3-morpholinopropyl)-5-oxo-1,5-dihydro-2H-dipyrido[1,2-a:2',3'-d]pyrimidine-3-carboxamide (6g). Yellow solid (68 mg, 64% yield). ^{1}H NMR (400 MHz, $CDCl_3$) δ 8.90 (d, *J* = 7.1 Hz, 1H), 7.69 (d, *J* = 6.8 Hz, 1H), 7.34 – 7.25 (m, 5H), 7.04 (t, *J* = 7.0 Hz, 1H), 4.64 (s, 2H), 3.74 (t, *J* = 4.5 Hz, 4H), 3.55 (dd, *J* = 11.8, 6.0 Hz, 2H), 3.05 (t, *J* = 7.9 Hz, 2H), 2.59 (s, 3H), 2.52 (s, 6H), 1.92 – 1.76 (m, 2H). ^{13}C NMR (151 MHz, $CDCl_3$) δ 156.1, 150.2, 137.1, 133.9, 130.2, 128.8, 126.2, 120.3, 114.3, 67.0, 53.8, 43.2, 32.2, 18.2. LRMS m/z 535.2 $[M + H]^+$. HPLC purity 100%, t_r = 2.05 min.

1-(4-bromophenethyl)-2-imino-10-methyl-N-(3-morpholinopropyl)-5-oxo-1,5-dihydro-2H-dipyrido[1,2-a:2',3'-d]pyrimidine-3-carboxamide (6h). Yellow solid (76 mg, 66% yield). ^{1}H NMR (400 MHz, $CDCl_3$) δ 8.90 (d, *J* = 6.8 Hz, 1H), 7.69 (d, *J* = 6.8 Hz, 1H), 7.45 (d, *J* = 8.2 Hz, 2H), 7.23 (d, *J* = 8.2 Hz, 2H), 7.04 (t, *J* = 7.0 Hz, 1H), 4.64 (s, 2H), 3.74 (t, *J* = 4.6 Hz, 4H), 3.55 (dd, *J* = 11.8, 6.2 Hz, 2H), 3.04 (t, *J* = 8.0 Hz, 2H), 2.59 (s, 3H), 2.58 – 2.47 (m, 6H), 1.84 (m, 2H). ^{13}C NMR (126 MHz, $CDCl_3$) δ 156.1, 150.2,

137.1, 133.9, 131.7, 130.6, 126.3, 120.3, 114.2, 67.0, 53.8, 43.1, 32.3, 18.2. LRMS m/z 581.1 $[M + H]^+$. HPLC purity 100%, t_r = 2.07 min.

1-(3-fluorophenethyl)-2-imino-10-methyl-N-(3-morpholinopropyl)-5-oxo-1,5-dihydro-2H-dipyrido[1,2-a:2',3'-d]pyrimidine-3-carboxamide (6i). Yellow solid (63 mg, 61% yield). ^{1}H NMR (400 MHz, $CDCl_3$) δ 8.89 (d, *J* = 6.3 Hz, 1H), 7.68 (d, *J* = 5.8 Hz, 1H), 7.29 (s, 1H), 7.19 – 7.00 (m, 2H), 6.93 (s, 1H), 4.67 (s, 1H), 3.74 (s, 4H), 3.55 (d, *J* = 4.5 Hz, 2H), 3.08 (d, *J* = 7.4 Hz, 2H), 2.60 (s, 3H), 2.52 (s, 6H), 1.84 (d, *J* = 5.8 Hz, 2H). ^{13}C NMR (126 MHz, $CDCl_3$) δ 163.9 162.0, 156.1, 155.5, 153.1, 150.2, 137.0, 133.9, 130.1, 126.2, 124.5, 120.3, 115.8, 115.6, 114.2, 113.6, 113.4, 67.0, 53.8, 43.1, 32.6, 18.1. LRMS m/z 519.3 $[M + H]^+$. HPLC purity 96.7%, t_r = 1.97 min.

1-(2-fluorophenethyl)-2-imino-10-methyl-N-(3-morpholinopropyl)-5-oxo-1,5-dihydro-2H-dipyrido[1,2-a:2',3'-d]pyrimidine-3-carboxamide (6j). Yellow solid (59 mg, 57% yield). ^{1}H NMR (400 MHz, $CDCl_3$) δ 11.20 (s, 1H), 9.06 (s, 1H), 8.89 (s, 1H), 7.67 (d, *J* = 5.5 Hz, 1H), 7.30 (s, 1H), 7.27 – 7.19 (m, 1H), 7.16 – 6.90 (m, 3H), 4.62 (s, 2H), 3.75 (t, *J* = 4.5 Hz, 4H), 3.55 (dd, *J* = 12.0, 6.2 Hz, 2H), 3.12 (s, 2H), 2.60 (s, 3H), 2.51 (s, 6H), 1.84 (dd, *J* = 13.2, 6.6 Hz, 2H). ^{13}C NMR (126 MHz, $CDCl_3$) δ 162.5, 160.5, 156.2, 150.1, 136.9, 134.2, 131.2, 128.7, 126.2, 124.4, 120.2, 115.5, 114.2, 67.0, 53.8, 41.9, 26.5, 17.9. LRMS m/z 519.3 $[M + H]^+$. HPLC purity 100%, t_r = 1.97 min.

1-(2-(diethylamino)ethyl)-2-imino-10-methyl-N-(3-morpholinopropyl)-5-oxo-1,5-dihydro-2H-dipyrido[1,2-a:2',3'-d]pyrimidine-3-carboxamide (6k). Yellow solid (59 mg, 60% yield). ^{1}H NMR (400 MHz, $CDCl_3$) δ 8.90 (d, *J* = 6.4 Hz, 1H), 7.66 (d, *J* = 6.6 Hz,

1H), 7.03 (t, *J* = 7.0 Hz, 1H), 4.45 (s, 2H), 3.73 (s, 4H), 3.52 (d, *J* = 5.9 Hz, 2H), 2.80 (t, *J* = 6.2 Hz, 2H), 2.68 (dd, *J* = 13.7, 6.7 Hz, 4H), 2.57 (s, 3H), 2.50 (s, 6H), 1.91 – 1.76 (m, 2H), 1.10 (t, *J* = 7.0 Hz, 6H). ^{13}C NMR (151 MHz, $CDCl_3$) δ 156.2, 155.5, 153.1, 150.1, 136.9, 136.5, 136.1, 133.9, 126.2, 125.6, 120.3, 116.6, 114.1, 67.0, 53.8, 47.8, 18.2, 12.2. LRMS m/z 496.3 $[M + H]^+$. HPLC purity 100%, t_r = 1.84 min.

2-imino-10-methyl-N-(3-morpholinopropyl)-5-oxo-1-(2-(thiophen-2-yl)ethyl)-1,5-dihydro-2H-dipyrido[1,2-a:2',3'-d]pyrimidine-3-carboxamide (6l). Yellow solid (64 mg, 63% yield). ^{1}H NMR (400 MHz, $CDCl_3$) δ 8.89 (d, *J* = 6.6 Hz, 1H), 7.66 (d, *J* = 6.8 Hz, 1H), 7.17 (s, 1H), 7.02 (t, *J* = 6.9 Hz, 1H), 6.95 (d, *J* = 4.8 Hz, 2H), 4.68 (s, 2H), 3.72 (t, *J* = 4.5 Hz, 4H), 3.53 (dd, *J* = 11.8, 6.2 Hz, 2H), 3.29 (t, *J* = 7.9 Hz, 2H), 2.60 (s, 3H), 2.50 (s, 6H), 1.93 – 1.76 (m, 2H). ^{13}C NMR (126 MHz, $CDCl_3$) δ 156.2, 155.4, 153.0, 150.2, 137.0, 134.2, 127.1, 126.2, 125.6, 124.0, 120.2, 114.3, 67.0, 53.8, 43.7, 27.0, 18.2. LRMS m/z 507.1 $[M + H]^+$. HPLC purity 100%, t_r = 1.93 min.

2-imino-10-methyl-1-(2-morpholinoethyl)-N-(3-morpholinopropyl)-5-oxo-1,5-dihydro-2H-dipyrido[1,2-a:2',3'-d]pyrimidine-3-carboxamide (6m). Yellow solid (73 mg, 72% yield). ^{1}H NMR (400 MHz, $CDCl_3$) δ 8.91 (d, *J* = 7.0 Hz, 1H), 7.68 (d, *J* = 6.8 Hz, 1H), 7.04 (t, *J* = 7.0 Hz, 1H), 4.57 (s, 2H), 3.75 (dt, *J* = 13.9, 4.5 Hz, 8H), 3.53 (dd, *J* = 12.0, 6.3 Hz, 2H), 2.76 (t, *J* = 7.0 Hz, 2H), 2.65 (s, 4H), 2.57 (s, 3H), 2.51 (s, 5H), 1.88 – 1.76 (m, 3H). ^{13}C NMR (151 MHz, $CDCl_3$) δ 156.2, 150.2, 137.1, 133.9, 126.3, 120.2, 114.3, 67.0, 54.0, 53.8, 18.2. LRMS m/z 510.3 $[M + H]^+$. HPLC purity 97.6%, t_r = 1.66 min.

2-imino-10-methyl-N-(3-morpholinopropyl)-5-oxo-1-(3-phenylpropyl)-1,5-dihydro-2H-dipyrido[1,2-a:2',3'-d]pyrimidine-3-carboxamide (6n). Yellow solid (69 mg, 67% yield). ^{1}H NMR (400 MHz, $CDCl_3$) δ 8.90 (d, *J* = 6.9 Hz, 1H), 8.71 (s, 1H), 7.68 (d, *J* = 6.7 Hz, 1H), 7.36 – 7.15 (m, 6H), 7.06 (t, *J* = 7.0 Hz, 1H), 4.55 (s, 2H), 3.74 (t, *J* = 4.4 Hz, 4H), 3.53 (s, 2H), 2.87 (t, *J* = 7.3 Hz, 2H), 2.63 – 2.47 (m, 6H), 2.42 (s, 3H), 2.21 – 2.09 (m, 2H), 1.89 – 1.79 (m, 2H). ^{13}C NMR (151 MHz, $CDCl_3$) δ 156.1, 155.5, 152.4, 150.1, 140.9, 137.2, 134.2, 128.7, 128.2, 126.1, 114.4, 66.8, 57.5, 53.7, 44.5, 42.2, 33.4, 27.7, 22.4, 17.9. LRMS m/z 515.2 $[M + H]^+$. HPLC purity 97.8%, t_r = 2.00 min.

2-imino-10-methyl-N-(3-morpholinopropyl)-5-oxo-1-(2-phenoxyethyl)-1,5-dihydro-2H-dipyrido[1,2-a:2',3'-d]pyrimidine-3-carboxamide (6o). Yellow solid (67 mg, 65% yield). ^{1}H NMR (400 MHz, CDCl3) δ 8.90 (s, 1H), 7.67 (d, *J* = 6.4 Hz, 1H), 7.28 (d, J = 6.5 Hz, 2H), 7.04 (t, *J* = 7.0 Hz, 0H), 6.94 (d, *J* = 8.1 Hz, 1H), 4.77 (s, 1H), 4.43 (t, *J* = 5.8 Hz, 2H), 3.88 – 3.64 (m, 4H), 3.55 (dd, *J* = 11.9, 6.1 Hz, 2H), 2.53 (s, 9H), 1.95 – 1.76 (m, 1H). ^{13}C NMR (126 MHz, $CDCl_3$) δ 156.1, 150.1, 137.0, 134.1, 129.4, 126.2, 120.9, 120.4, 115.0, 114.8, 113.9, 67.0, 53.8, 18.0. LRMS m/z 517.2 $[M + H]^+$. HPLC purity 100%, t_r = 1.94 min.

2-imino-10-methyl-N,1-bis(3-morpholinopropyl)-5-oxo-1,5-dihydro-2H-dipyrido[1,2-a:2',3'-d]pyrimidine-3-carboxamide (6p). Yellow solid (60 mg, 57% yield). ^{1}H NMR (400 MHz, $CDCl_3$) δ 8.89 (d, *J* = 6.8 Hz, 1H), 7.66 (d, *J* = 6.7 Hz, 1H), 7.03 (t, *J* = 7.0 Hz, 1H), 4.43 (s, 2H), 3.75 (dd, *J* = 14.8, 10.6 Hz, 8H), 3.62 – 3.39 (m, 2H), 2.56 (s, 4H), 2.49 (s, 12H), 2.12 – 1.92 (m, 4H), 1.89 – 1.75 (m, 2H). ^{13}C NMR (151

MHz, $CDCl_3$) δ 156.2, 153.0, 150.1, 137.0, 133.9, 126.2, 120.0, 114.2, 67.0, 53.7, 40.5, 23.9, 18.1. LRMS m/z 524.2 $[M + H]^+$. HPLC purity 98.2%, t_r = 1.69 min.

1-benzyl-2-imino-10-methyl-N-(3-morpholinopropyl)-5-oxo-1,5-dihydro-2H-dipyrido[1,2-a:2',3'-d]pyrimidine-3-carboxamide (6q). ^{1}H NMR (500 MHz, $CDCl_3$) δ 8.90 (d, *J* = 6.6 Hz, 1H), 7.63 (d, *J* = 6.6 Hz, 1H), 7.31 (s, 4H), 7.02 (t, *J* = 6.9 Hz, 1H), 5.68 (s, 2H), 3.82 – 3.64 (m, 4H), 3.53 – 3.37 (m, 2H), 2.46 (s, 9H), 1.88 – 1.69 (m, 2H).^{13}C NMR (126 MHz, CDCl3) δ 156.2, 153.3, 150.2, 137.0, 134.3, 128.9, 127.6, 126.5, 125.9, 124.7, 120.4, 114.4, 67.0, 53.8, 45.7, 18.1. LRMS m/z 487.4 $[M + H]^+$. HPLC purity 97.6%, t_r = 2.07 min.

2-imino-10-methyl-N-(3-morpholinopropyl)-5-oxo-1-(pyridin-4-ylmethyl)-1,5-dihydro-2H-dipyrido[1,2-a:2',3'-d]pyrimidine-3-carboxamide (6r). ^{1}H NMR (400 MHz, $CDCl_3$) δ 8.87 (d, *J* = 7.0 Hz, 1H), 8.51 (d, *J* = 4.7 Hz, 2H), 7.62 (d, J = 6.8 Hz, 1H), 7.24 (d, *J* = 4.1 Hz, 2H), 7.02 (t, *J* = 7.0 Hz, 1H), 5.70 (s, 2H), 3.70 (t, *J* = 4.5 Hz, 4H), 3.50 (d, *J* = 5.4 Hz, 2H), 2.49 (s, 6H), 2.38 (s, 3H), 1.79 (dd, *J* = 12.8, 6.3 Hz, 2H). LRMS m/z 488.2 $[M + H]^+$. HPLC purity 100%, t_r = 1.95 min.

2-imino-10-methyl-N-(3-morpholinopropyl)-5-oxo-1-phenyl-1,5-dihydro-2H-dipyrido[1,2-a:2',3'-d]pyrimidine-3-carboxamide (6s). Yellow solid (75 mg, 79% yield). ^{1}H NMR (400 MHz, $CDCl_3$) δ 10.96 (s, 1H), 9.11 (s, 1H), 8.87 (d, *J* = 7.2 Hz, 1H), 7.63 (t, *J* = 7.5 Hz, 2H), 7.56 (d, *J* = 7.4 Hz, 1H), 7.54 – 7.47 (m, 1H), 7.24 (s, 1H), 6.96 (t, *J* = 7.0 Hz, 1H), 6.65 (s, 1H), 3.92 – 3.59 (m, 4H), 3.48 (dd, *J* = 12.7, 6.8 Hz, 2H), 2.42 (t, *J* = 7.3 Hz, 6H), 1.99 (s, 3H), 1.79 (m, 2H). ^{13}C NMR (126 MHz, $CDCl_3$) δ 163.7,

156.3, 153.8, 150.0, 136.9, 135.6, 134.4, 130.4, 129.4, 126.0, 120.0, 114.3, 96.0, 67.0, 56.6, 53.7, 37.7, 26.5, 17.1. LRMS m/z 473.2 $[M + H]^+$. HPLC purity 98.2%, t_r = 1.92 min.

1-cyclohexyl-2-imino-10-methyl-N-(3-morpholinopropyl)-5-oxo-1,5-dihydro-2H-dipyrido[1,2 -a:2',3'-d]pyrimidine-3-carboxamide (6t). Yellow solid (63 mg, 66% yield). ^{1}H NMR (400 MHz, $CDCl_3$) δ 8.86 (d, *J* = 6.9 Hz, 1H), 8.46 (s, 1H), 7.64 (d, *J* = 6.8 Hz, 1H), 7.00 (t, *J* = 7.0 Hz, 1H), 5.36 (s, 1H), 3.73 (t, *J* = 4.5 Hz, 4H), 3.52 (dd, *J* = 11.1, 5.9 Hz, 2H), 2.81 (s, 2H), 2.62 (s, 3H), 2.59 – 2.46 (m, 5H), 1.95 (d, *J* = 13.4 Hz, 2H), 1.87 – 1.77 (m, 5H), 1.52 (m, 2H), 1.31 (m, 2H). ^{13}C NMR (151 MHz, $CDCl_3$) δ 156.4, 149.4, 136.6, 134.1, 126.0, 120.8, 114.0, 67.0, 53.8, 28.9, 26.8, 25.8, 18.6. LRMS m/z 479.5 $[M + H]^+$. HPLC purity 97.5%, t_r = 2.17 min.

2-imino-1,10-dimethyl-N-(3-morpholinopropyl)-5-oxo-1,5-dihydro-2H-dipyrido[1,2-a:2',3'-d]pyrimidine-3-carboxamide (6u). Yellow solid (66 mg, 80% yield). ^{1}H NMR (400 MHz, $CDCl_3$) δ 11.17 (s, 1H), 9.08 (s, 1H), 8.89 (d, *J* = 6.4 Hz, 1H), 7.64 (d, *J* = 6.7 Hz, 1H), 7.00 (dd, *J* = 9.5, 4.4 Hz, 1H), 4.35 (s, 2H), 3.72 (t, *J* = 4.5 Hz, 4H), 3.52 (dd, *J* = 12.1, 6.3 Hz, 2H), 2.56 (s, 3H), 2.48 (s, 5H), 1.90 – 1.74 (m, 4H). ^{13}C NMR (151 MHz, $CDCl_3$) δ 156.2, 150.1, 136.8, 134.0, 126.1, 120.1, 114.1, 67.0, 53.8, 43.6, 20.0, 18.0, 11.7. LRMS m/z 439.1 $[M + H]^+$. HPLC purity 96.1%, t_r = 1.81 min.

2-imino-1-isopropyl-10-methyl-N-(3-morpholinopropyl)-5-oxo-1,5-dihydro-2H-dipyrido[1,2-a:2',3'-d]pyrimidine-3-carboxamide (6v). Yellow solid (71 mg, 81% yield). ^{1}H NMR (600 MHz, $CDCl_3$) δ 8.84 (d, *J* = 7.0 Hz, 1H), 7.61 (d, *J* = 6.8 Hz, 1H),

6.97 (t, *J* = 7.0 Hz, 1H), 5.85 (s, 1H), 3.70 (t, *J* = 4.5 Hz, 4H), 3.50 (dd, *J* = 11.8, 6.2 Hz, 2H), 2.57 (s, 3H), 2.50 (m, 6H), 1.85 – 1.75 (m, 2H), 1.69 (d, *J* = 7.1 Hz, 6H). ^{13}C NMR (126 MHz, $CDCl_3$) δ 156.4, 149.6, 136.6, 134.1, 126.0, 120.9, 114.0, 67.0, 53.8, 46.9, 19.5, 18.5. LRMS m/z 439.1 $[M + H]^+$. HPLC purity 97.9%, t_r = 1.80 min.

2-imino-10-methyl-N-(3-morpholinopropyl)-5-oxo-1-propyl-1,5-dihydro-2H-dipyrido[1,2-a:2',3'-d]pyrimidine-3-carboxamide (6w). Yellow solid (74 mg, 84% yield). ^{1}H NMR (400 MHz, $CDCl_3$) δ 11.20 (s, 1H), 9.07 (s, 1H), 8.91 (s, 1H), 7.67 (d, *J* = 6.5 Hz, 1H), 7.03 (s, 2H), 3.74 (s, 4H), 3.54 (d, *J* = 5.8 Hz, 2H), 2.58 (s, 3H), 2.50 (s, 6H), 1.83 (d, *J* = 7.5 Hz, 4H), 1.09 (s, 3H). ^{13}C NMR (126 MHz, $CDCl_3$) δ 156.2, 155.6, 153.0, 150.1, 136.8, 134.0, 126.1, 120.2, 114.1, 67.0, 53.8, 43.6, 20.0, 18.0, 11.7. LRMS m/z 439.1 $[M + H]^+$. HPLC purity 100%, t_r = 1.82 min.

2-imino-10-methyl-N-(3-morpholinopropyl)-5-oxo-1-(prop-2-yn-1-yl)-1,5-dihydro-2H-dipyrido[1,2-a:2',3'-d]pyrimidine-3-carboxamide (6x). Yellow solid (64 mg, 74% yield). ^{1}H NMR (400 MHz, $CDCl_3$) δ 10.21 (t, *J* = 4.5 Hz, 1H), 9.07 – 8.99 (m, 1H), 8.95 (s, 1H), 8.09 (d, *J* = 1.0 Hz, 1H), 7.77 – 7.69 (m, 1H), 7.11 (t, *J* = 7.0 Hz, 1H), 3.80 – 3.71 (m, 4H), 3.65 (m, 2H), 2.69 (s, 3H), 2.54 (m, 9H), 1.92 (m, 2H). ^{13}C NMR (151 MHz, $CDCl_3$) δ 162.8, 157.3, 149.5, 144.9, 143.6, 142.2, 136.6, 134.5, 125.9, 117.4, 114.6, 108.7, 99.9, 66.9, 56.3, 53.7, 37.6, 26.4, 17.9, 14.3. LRMS m/z 435.1 $[M + H]^+$. HPLC purity 99.4%, t_r = 1.95 min.

1-(2-(1H-indol-3-yl)ethyl)-2-imino-10-methyl-N-(3-morpholinopropyl)-5-oxo-1,5-dihydro-2H-dipyrido[1,2-a:2',3'-d]pyrimidine-3-carboxamide (6y). Yellow solid (61

mg, 57% yield). ^{1}H NMR (400 MHz, $CDCl_3$) δ 8.90 (d, *J* = 6.9 Hz, 1H), 8.30 (s, 1H), 7.77 (d, *J* = 7.4 Hz, 1H), 7.64 (d, *J* = 7.0 Hz, 1H), 7.40 (d, *J* = 8.1 Hz, 1H), 7.23 (t, *J* = 7.4 Hz, 1H), 7.17 (t, *J* = 7.3 Hz, 1H), 7.11 (s, 1H), 7.02 (t, *J* = 7.0 Hz, 1H), 4.73 (s, 2H), 3.75 (t, *J* = 4.5 Hz, 4H), 3.55 (dd, *J* = 12.0, 6.1 Hz, 2H), 3.25 (t, *J* = 7.7 Hz, 2H), 2.53 (s, 9H), 1.88 – 1.81 (m, 2H). ^{13}C NMR (151 MHz, DMSO-d_6) δ 166.8, 156.2, 155.9, 153.3, 150.4, 140.13, 138.3, 136.7, 133.5, 130.4, 127.8, 127.4, 126.3, 123.0, 121.4, 119.6, 119.5, 119.3, 118.7, 116.1, 115.3, 112.3, 111.8, 93.9, 66.7, 56.7, 53.9, 42.8, 38.1, 26.2, 22.7, 17.9. LRMS m/z 540.3 $[M + H]^+$. HPLC purity 100%, t_r = 1.90 min.

1-(4-chlorophenyl)-2-imino-10-methyl-N-(3-morpholinopropyl)-5-oxo-1,5-dihydro-2H-dipyrido[1,2-a:2',3'-d]pyrimidine-3-carboxamide (6z). ^{1}H NMR (400 MHz, $CDCl_3$) δ 10.88 (s, 1H), 9.11 (s, 1H), 8.91 (d, *J* = 6.8 Hz, 1H), 7.64 (d, *J* = 8.5 Hz, 2H), 7.58 (d, *J* = 6.8 Hz, 1H), 7.24 (d, *J* = 8.5 Hz, 2H), 7.02 (t, *J* = 7.0 Hz, 1H), 3.75 (t, *J* = 4.3 Hz, 4H), 3.51 (q, *J* = 6.5 Hz, 2H), 2.51 (d, *J* = 4.9 Hz, 6H), 2.07 (s, 3H), 1.91 – 1.77 (m, 2H). ^{13}C NMR (126 MHz, $CDCl_3$) δ 163.7, 156.1, 153.7, 150.0, 137.0, 135.4, 134.4, 134.1, 131.0, 130.7, 126.1, 120.0, 114.5, 96.1, 66.7, 56.6, 53.6, 37.7, 26.3, 17.3. LRMS m/z 507.1 $[M + H]^+$. HPLC purity 96.2%, t_r = 2.01 min.

2-imino-10-methyl-5-oxo-N-(3-phenylpropyl)-1-(2-(thiophen-2-yl)ethyl)-1,5-dihydro-2H-dipyrido[1,2-a:2',3'-d]pyrimidine-3-carboxamide (**6la**). Yellow solid (73 mg, 73% yield). ^{1}H NMR (400 MHz, $CDCl_3$) δ 11.18 (s, 1H), 9.06 (s, 1H), 8.92 (d, *J* = 7.0 Hz, 1H), 7.69 (d, *J* = 6.6 Hz, 1H), 7.27 (m, 7H), 7.05 (t, *J* = 6.9 Hz, 1H), 7.02 – 6.92 (m, 2H), 4.63 (s, 2H), 3.51 (dd, *J* = 12.7, 6.6 Hz, 2H), 3.30 (t, *J* = 7.9 Hz, 2H), 2.76 (t, *J* = 7.6 Hz, 2H), 2.62 (s, 3H), 2.09 – 1.90 (m, 2H). ^{13}C NMR (151 MHz, $CDCl_3$) δ 156.3, 150.1,

141.8, 137.1, 134.2, 128.5, 127.2, 126.2, 125.9, 125.7, 124.3, 120.1, 114.4, 43.6, 39.2, 33.5, 31.2, 27.0, 18.3. LRMS m/z 498.1 $[M + H]^+$. HPLC purity 99.5%, t_r = 2.25 min.

2-imino-10-methyl-N-(2-morpholinoethyl)-5-oxo-1-(2-(thiophen-2-yl)ethyl)-1,5-dihydro-2H-dipyrido[1,2-a:2',3'-d]pyrimidine-3-carboxamide (6lb). ^{1}H NMR (400 MHz, $CDCl_3$) δ 11.13 (s, 1H), 9.08 (s, 1H), 8.93 (s, 1H), 7.69 (s, 1H), 7.13 (s, 1H), 7.03 (m, 1H), 4.63 (m, 2H), 4.05 (s, 1H), 3.05 (t, *J* = 7.7 Hz, 2H), 2.60 (s, 3H), 2.02 (s, 2H), 1.77 (s, 2H), 1.65 (s, 2H), 1.45 (m, 4H). ^{13}C NMR (126 MHz, $CDCl_3$) δ 156.3, 155.3, 150.2, 137.1, 134.2, 127.2, 126.2, 125.6, 124.1, 120.3, 114.3, 67.1, 57.3, 53.5, 43.6, 36.6, 27.0, 18.2. LRMS m/z 493.1 $[M + H]^+$. HPLC purity 97.5%, t_r = 1.90 min.

2-imino-10-methyl-N-(2-(4-methylpiperazin-1-yl)ethyl)-5-oxo-1-(2-(thiophen-2-yl)ethyl)-1,5-dihydro-2H-dipyrido[1,2-a:2',3'-d]pyrimidine-3-carboxamide (**6lc**). Yellow solid (69 mg, 68% yield). ^{1}H NMR (400 MHz, $CDCl_3$) δ 8.92 (d, J = 6.6 Hz, 1H), 7.69 (d, J = 6.8 Hz, 1H), 7.20 (s, 1H), 7.05 (t, J = 7.0 Hz, 1H), 6.98 (d, J = 6.2 Hz, 2H), 4.69 (s, 2H), 3.60 (d, J = 4.5 Hz, 2H), 3.31 (t, J = 7.9 Hz, 2H), 2.66 (d, J = 6.3 Hz, 3H), 2.62 (s, 5H), 2.60 – 2.42 (m, 5H), 2.34 (s, 3H). ^{13}C NMR (126 MHz, $CDCl_3$) δ 156.3, 150.2, 137.0, 134.2, 127.1, 126.1, 125.6, 124.1, 114.3, 56.8, 55.1, 52.9, 46.0, 43.6, 36.8, 27.0, 18.2. LRMS m/z 506.2 $[M + H]^+$. HPLC purity 95.6%, t_r = 1.88 min.

2-imino-10-methyl-5-oxo-N-phenethyl-1-(2-(thiophen-2-yl)ethyl)-1,5-dihydro-2H-dipyrido[1,2-a:2',3'-d]pyrimidine-3-carboxamide (6ld). ^{1}H NMR (400 MHz, $CDCl_3$) δ 11.17 (s, 1H), 8.98 (s, 1H), 8.88 (d, *J* = 6.1 Hz, 1H), 7.67 (d, *J* = 6.8 Hz, 1H), 7.44 – 7.17 (m, 6H), 6.99 (m, 3H), 4.60 (s, 2H), 3.73 (dd, *J* = 13.3, 6.9 Hz, 2H), 3.27 (t, *J* = 8.0 Hz,

2H), 2.97 (t, *J* = 7.3 Hz, 2H), 2.60 (s, 3H). ^{13}C NMR (126 MHz, $CDCl_3$) δ 156.2, 155.0, 152.7, 150.1, 139.5, 137.1, 134.1, 128.9, 128.5, 127.2, 126.3, 125.6, 124.2, 120.1, 114.4, 43.5, 41.2, 35.9, 26.9, 18.2. LRMS m/z 502.1 $[M + H]^+$. HPLC purity 100%, t_r = 2.20 min.

***N*-(4-fluorophenethyl)-2-imino-10-methyl-5-oxo-1-(2-(thiophen-2-yl)ethyl)-1,5-dihydro-2H-dipyrido[1,2-a:2',3'-d]pyrimidine-3-carboxamide (6le).** ^{1}H NMR (400 MHz, $CDCl_3$) δ 8.93 (d, *J* = 6.7 Hz, 1H), 7.70 (d, *J* = 6.6 Hz, 1H), 7.28 – 7.19 (m, 3H), 7.11 – 6.94 (m, 5H), 4.66 (s, 2H), 3.71 (dd, *J* = 13.2, 6.8 Hz, 2H), 3.30 (t, *J* = 7.9 Hz, 2H), 2.94 (t, *J* = 7.3 Hz, 2H), 2.63 (s, 3H). ^{13}C NMR (126 MHz, $CDCl_3$) δ 164.4, 162.6, 160.6, 156.2, 155.1, 152.7, 150.2, 140.0, 137.2, 135.1, 134.2, 130.2, 128.6, 127.2, 126.2, 125.7, 124.2, 119.8, 115.3, 115.2, 114.4, 43.6, 41.2, 35.0, 26.9, 18.2. LRMS m/z 484.1 $[M + H]^+$. HPLC purity 100%, t_r = 2.20 min.

2-imino-N-(4-methoxyphenethyl)-10-methyl-5-oxo-1-(2-(thiophen-2-yl)ethyl)-1,5-dihydro-2H-dipyrido[1,2-a:2',3'-d]pyrimidine-3-carboxamide (**6lf**). Yellow solid (52 mg, 51% yield). ^{1}H NMR (400 MHz, $CDCl_3$) δ 11.16 (s, 1H), 9.06 (s, 1H), 8.91 (s, 1H), 7.68 (d, *J* = 6.7 Hz, 1H), 7.22 (d, *J* = 8.3 Hz, 3H), 7.04 (t, *J* = 7.0 Hz, 1H), 6.99 (s, 1H), 6.96 (d, *J* = 2.9 Hz, 1H), 6.89 (d, *J* = 8.5 Hz, 2H), 4.59 (s, 2H), 3.82 (s, 3H), 3.69 (dd, *J* = 13.2, 6.9 Hz, 2H), 3.28 (t, *J* = 8.0 Hz, 2H), 2.91 (t, *J* = 7.3 Hz, 2H), 2.61 (s, 3H). ^{13}C NMR (126 MHz, CDCl3) δ 158.2, 156.2, 155.1, 152.8, 150.1, 137.1, 134.1, 131.5, 129.8, 127.2, 126.2, 125.6, 124.2, 120.1, 114.4, 114.0, 55.3, 43.5, 41.4, 35.0, 27.0, 18.2. LRMS m/z 514.2 $[M + H]^+$. HPLC purity 98.1%, t_r = 2.17 min.

N-benzyl-2-imino-10-methyl-5-oxo-1-(2-(thiophen-2-yl)ethyl)-1,5-dihydro-2H-dipyrido[1,2-a:2',3'-d]pyrimidine-3-carboxamide (**6lg**). Yellow solid (64 mg, 68% yield). ^{1}H NMR (400 MHz, $CDCl_3$) δ 11.56 (s, 1H), 9.10 (s, 1H), 8.91 (s, 1H), 7.69 (d, *J* = 6.7 Hz, 1H), 7.39 (dt, *J* = 15.0, 7.5 Hz, 4H), 7.30 (d, *J* = 7.2 Hz, 1H), 7.21 (d, *J* = 4.7 Hz, 1H), 7.05 (t, *J* = 6.9 Hz, 1H), 7.02 – 6.92 (m, 2H), 4.69 (d, *J* = 5.2 Hz, 2H), 4.60 (s, 1H), 3.28 (t, *J* = 8.1 Hz, 2H), 2.62 (s, 3H). ^{13}C NMR (126 MHz, $CDCl_3$) δ 155.8, 154.5, 149.7, 142.7, 136.7, 133.7, 128.2, 127.3, 126.8, 125.7, 125.2, 123.9, 119.4, 114.0, 43.2, 26.47, 17.8. LRMS m/z 470.0 $[M + H]^+$. HPLC purity 100%, t_r = 2.17 min.

2-imino-10-methyl-5-oxo-N-((tetrahydrofuran-2-yl)methyl)-1-(2-(thiophen-2-yl)ethyl)-1,5-dihydro-2H-dipyrido[1,2-a:2',3'-d]pyrimidine-3-carboxamide (**6lh**). Yellow solid (73 mg, 79% yield). ^{1}H NMR (400 MHz, $CDCl_3$) δ 8.92 (d, *J* = 6.9 Hz, 1H), 8.81 (s, 1H), 7.69 (d, *J* = 6.6 Hz, 1H), 7.21 (d, *J* = 4.7 Hz, 1H), 7.05 (t, *J* = 6.9 Hz, 1H), 7.02 – 6.91 (m, 2H), 4.63 (s, 2H), 4.13 (d, *J* = 3.7 Hz, 1H), 3.96 (dd, *J* = 14.3, 7.0 Hz, 1H), 3.82 (td, *J* = 14.1, 5.5 Hz, 2H), 3.47 – 3.35 (m, 1H), 3.29 (t, *J* = 8.0 Hz, 2H), 2.62 (s, 3H), 2.15 – 2.02 (m, 1H), 1.95 (dd, *J* = 13.8, 6.7 Hz, 2H), 1.75 – 1.59 (m, 1H). ^{13}C NMR (126 MHz, $CDCl_3$) δ 164.7, 156.2, 155.1, 152.8, 150.2, 140.2, 137.1, 134.2, 127.2, 126.2, 125.6, 124.2, 120.1, 114.4, 95.7, 77.9, 68.3, 43.7, 29.0, 27.0, 26.0, 18.2. LRMS m/z 464.0 $[M + H]^+$. HPLC purity 100%, t_r = 1.99 min.

N-cyclohexyl-2-imino-10-methyl-5-oxo-1-(2-(thiophen-2-yl)ethyl)-1,5-dihydro-2H-dipyrido[1,2-a:2',3'-d]pyrimidine-3-carboxamide (**6li**). Yellow solid (69 mg, 75% yield). ^{1}H NMR (400 MHz, $CDCl_3$) δ 8.92 (s, 1H), 7.69 (d, *J* = 6.7 Hz, 1H), 7.22 (s, 1H), 7.05 (t, *J* = 7.0 Hz, 1H), 6.98 (d, *J* = 8.6 Hz, 1H), 4.63 (s, 2H), 4.02 (s, 1H), 3.29 (t, *J* = 8.1

Hz, 2H), 2.62 (s, 2H), 2.01 (s, 1H), 1.75 (s, 1H), 1.67 – 1.59 (m, 1H), 1.41 (m, 3H). ^{13}C NMR (126 MHz, $CDCl_3$) δ 156.2, 155.3, 152.8, 150.1, 140.3, 137.0, 134.2, 127.2, 126.2, 125.6, 124.1, 120.5, 114.3, 48.3, 43.6, 33.0, 27.0, 25.8, 24.7, 18.2. LRMS m/z 462.1 $[M + H]^+$. HPLC purity 98.3%, t_r = 2.28 min.

N-(2-hydroxyethyl)-2-imino-10-methyl-5-oxo-1-(2-(thiophen-2-yl)ethyl)-1,5-dihydro-2H-dipyrido[1,2-a:2',3'-d]pyrimidine-3-carboxamide (6lj). Yellow solid (69 mg, 81% yield). ^{1}H NMR (500 MHz, $CDCl_3$) δ 8.86 (d, *J* = 5.5 Hz, 1H), 7.68 (d, *J* = 6.7 Hz, 1H), 7.20 (d, *J* = 4.9 Hz, 1H), 7.04 (t, *J* = 6.9 Hz, 1H), 7.00 – 6.95 (m, 1H), 6.93 (d, *J* = 3.0 Hz, 1H), 4.55 (s, 2H), 3.96 – 3.82 (m, 2H), 3.64 (d, *J* = 4.7 Hz, 2H), 3.24 (s, 2H), 2.58 (s, 3H). ^{13}C NMR (126 MHz, $CDCl_3$) δ 156.1, 154.9, 152.7, 150.1, 137.3, 134.1, 127.2, 126.2, 125.6, 124.2, 114.5, 62.9, 58.5, 43.6, 43.1, 26.9, 18.4, 18.2. LRMS m/z 424.1 $[M + H]^+$. HPLC purity 100%, t_r = 1.83 min.

2-imino-9-methyl-N-(3-morpholinopropyl)-5-oxo-1-(2-(thiophen-2-yl)ethyl)-1,5-dihydro-2H-dipyrido[1,2-a:2',3'-d]pyrimidine-3-carboxamide (6lk). ^{1}H NMR (400 MHz, $CDCl_3$) δ 8.38 (d, *J* = 6.2 Hz, 1H), 7.65 (d, *J* = 8.6 Hz, 1H), 7.47 (d, *J* = 8.9 Hz, 1H), 7.41 (dd, *J* = 9.1, 2.0 Hz, 1H), 7.20 (d, *J* = 5.1 Hz, 1H), 7.13 (d, *J* = 9.1 Hz, 1H), 6.88 (d, *J* = 3.3 Hz, 1H), 3.83 (q, *J* = 6.6 Hz, 2H), 3.78 – 3.67 (m, 4H), 3.59 – 3.47 (m, 2H), 3.26 (t, *J* = 6.7 Hz, 4H), 2.50 (s, 5H), 2.43 (s, 3H), 2.27 (s, 2H), 1.81 (d, *J* = 6.6 Hz, 2H). ^{13}C NMR (126 MHz, $CDCl_3$) δ 172.6, 162.3, 161.0, 155.7, 153.3, 142.0, 141.0, 138.4, 127.2, 126.5, 125.3, 125.9, 124.4, 124.9, 124.7, 121.5, 94.5, 67.0, 53.8, 52.4, 43.2, 30.8, 27.2, 18.2, 17.8. LRMS m/z 507.1 $[M + H]^+$. HPLC purity 100%, t_r = 1.92 min.

2-imino-N-(3-morpholinopropyl)-5-oxo-1-(2-(thiophen-2-yl)ethyl)-1,5-dihydro-2H-dipyrido[1,2-a:2',3'-d]pyrimidine-3-carboxamide (6ll). Yellow solid (58 mg, 59% yield). ^{1}H NMR (400 MHz, $CDCl_3$) δ 9.00 (s, 1H), 7.80 (t, *J* = 7.3 Hz, 1H), 7.56 (d, *J* = 8.7 Hz, 1H), 7.19 (s, 1H), 7.12 (s, 1H), 6.96 (s, 2H), 4.68 (s, 2H), 3.74 (t, *J* = 4.5 Hz, 4H), 3.55 (d, *J* = 5.6 Hz, 2H), 3.29 (t, *J* = 7.6 Hz, 2H), 2.52 (s, 6H), 1.94 – 1.78 (m, 2H). ^{13}C NMR (126 MHz, $CDCl_3$) δ 155.8, 150.7, 138.1, 128.1, 127.0, 126.3, 126.0, 125.6, 124.0, 120.4, 114.7, 67.0, 53.8, 43.3, 27.2. LRMS m/z 493.2 $[M + H]^+$. HPLC purity 100%, t_r = 1.85 min.

General synthetic procedure for compound 7. A mixture of ethyl 2-cyanoacetate (113 mg, 1.0 mmol, 2.0 eq) and corresponding imine intermediate **4** (0.5 mmol, 1.0 eq) was refluxed in $CHCl_3$ overnight in the presence of a catalytic amount of piperidine. The yellow mixture was concentrated in vacuum. The crude product **7** was purified by recrystallization from EtOH as a yellow solid.

ethyl 2-imino-1-isopropyl-10-methyl-5-oxo-1,5-dihydro-2H-dipyrido[1,2-a:2',3'-d]pyrimidine-3-carboxylate (7a). Yellow solid (152 mg, 89% yield). ^{1}H NMR (400 MHz, $CDCl_3$) δ 9.69 (s, 1H), 8.85 (dd, *J* = 7.1, 0.7 Hz, 1H), 8.64 (s, 1H), 7.64 (d, *J* = 6.8 Hz, 1H), 6.99 (t, *J* = 7.0 Hz, 1H), 6.09 (dt, *J* = 13.9, 6.9 Hz, 1H), 4.35 (q, *J* = 7.1 Hz, 2H), 2.63 (d, *J* = 12.6 Hz, 3H), 1.73 (t, *J* = 7.6 Hz, 6H), 1.40 (t, *J* = 7.1 Hz, 3H). ^{13}C NMR (126 MHz, $CDCl_3$) δ 165.7, 157.2, 156.4, 155.0, 150. 2, 137.4, 137.0, 134.3, 126.0, 114.1, 114.9, 95.3, 61.0, 58.4, 46.7, 19.5, 18.7, 18.4, 14.3. LRMS m/z 341.1 $[M + H]^+$. HPLC purity 97.7%, t_r = 2.09 min.

ethyl 2-imino-10-methyl-5-oxo-1-propyl-1,5-dihydro-2H-dipyrido[1,2-a:2',3'-d]pyrimidine-3-carboxylate (7b). Yellow solid (148 mg, 87% yield). ^{1}H NMR (400 MHz, $CDCl_3$) δ 9.51 (s, 1H), 8.86 (d, *J* = 7.1 Hz, 1H), 8.66 (s, 1H), 7.66 (d, *J* = 6.8 Hz, 1H), 7.01 (t, *J* = 7.0 Hz, 1H), 4.58 – 4.46 (m, 2H), 4.36 (q, *J* = 7.1 Hz, 2H), 2.57 (s, 3H), 1.83 (dd, *J* = 15.2, 7.5 Hz, 2H), 1.41 (t, *J* = 7.1 Hz, 3H), 1.05 (t, *J* = 7.4 Hz, 3H). ^{13}C NMR (126 MHz, $CDCl_3$) δ 165.1, 155.8, 153.9, 150.4, 136.9, 136.7, 133.7, 125.6, 113.5, 60.5, 43.5, 19.7, 17.5, 13.9, 11.2. LRMS m/z 341.0 $[M + H]^+$. HPLC purity 100%, t_r = 2.08 min.

ethyl 2-imino-10-methyl-5-oxo-1-phenethyl-1,5-dihydro-2H-dipyrido[1,2-a:2',3'-d]pyrimidine-3-carboxylate (7c). Yellow solid (176 mg, 87% yield). ^{1}H NMR (400 MHz, $CDCl_3$) δ 9.60 (s, 1H), 8.86 (d, *J* = 7.1 Hz, 1H), 8.66 (s, 1H), 7.67 (d, *J* = 6.8 Hz, 1H), 7.38 (d, *J* = 7.3 Hz, 2H), 7.31 (t, *J* = 7.5 Hz, 2H), 7.22 (d, *J* = 7.3 Hz, 1H), 7.02 (t, *J* = 7.0 Hz, 1H), 4.84 – 4.73 (m, 2H), 4.38 (q, *J* = 7.1 Hz, 2H), 3.14 – 3.00 (m, 2H), 2.60 (s, 3H), 1.42 (t, *J* = 7.1 Hz, 3H). ^{13}C NMR (126 MHz, $CDCl_3$) δ 165.1, 155.8, 155.3, 153.8, 150.4, 139.0, 136.8, 133.7, 128.5, 127.9, 125.7, 113.6, 113.4, 94.2, 60.6, 43.2, 32.4, 17.7, 13.9. LRMS m/z 403.1 $[M + H]^+$. HPLC purity 100%, t_r = 2.24 min.

ethyl 1-(4-chlorophenethyl)-2-imino-10-methyl-5-oxo-1,5-dihydro-2H-dipyrido[1,2-a:2',3'-d]pyrimidine-3-carboxylate (7d). Yellow solid (183 mg, 84% yield). ^{1}H NMR (400 MHz, $CDCl_3$) δ 9.56 (s, 1H), 8.85 (d, *J* = 7.1 Hz, 1H), 8.63 (s, 1H), 7.67 (d, *J* = 6.8 Hz, 1H), 7.36 – 7.18 (m, 4H), 7.02 (d, *J* = 7.0 Hz, 1H), 4.77 – 4.66 (m, 2H), 4.36 (q, *J* = 7.1 Hz, 2H), 3.03 (dd, *J* = 9.2, 6.7 Hz, 2H), 2.56 (s, 3H), 1.41 (t, *J* = 7.1 Hz, 3H). ^{13}C NMR (126 MHz, $CDCl_3$) δ 165.5, 156.1, 155.7, 154.2, 150.9, 137.9, 137.5, 137.3, 134.0,

132.0, 130.3, 128.5, 126.2, 114.2, 113.8, 94.6, 61.1, 43.4, 32.2, 18.1, 14.3. LRMS m/z 437.0 $[M + H]^+$. HPLC purity 95.0%, t_r = 2.34 min.

ethyl 2-imino-10-methyl-1-(4-methylphenethyl)-5-oxo-1,5-dihydro-2H-dipyrido[1,2-a:2',3'-d]pyrimidine-3-carboxylate (7e). Yellow solid (158 mg, 76% yield). ^{1}H NMR (600 MHz, $CDCl_3$) δ 9.57 (s, 1H), 8.85 (d, *J* = 6.7 Hz, 1H), 8.65 (s, 1H), 7.65 (d, *J* = 6.8 Hz, 1H), 7.30 – 7.21 (m, 3H), 7.11 (d, *J* = 7.7 Hz, 2H), 6.99 (t, *J* = 7.0 Hz, 1H), 4.81 – 4.68 (m, 2H), 4.36 (q, *J* = 7.1 Hz, 2H), 3.08 – 2.97 (m, 2H), 2.59 (s, 3H), 2.30 (s, 3H), 1.40 (t, *J* = 7.1 Hz, 3H). ^{13}C NMR (126 MHz, $CDCl_3$) δ 165.6, 156.3, 155.9, 154.3, 150.9, 137.3, 136.4, 135.7, 134.2, 129.1, 128.9, 126.2, 114.0, 94.7, 61.0, 43.9, 32.5, 21.0, 18.2, 14.3. LRMS m/z 417.2 $[M + H]^+$. HPLC purity 100%, t_r = 2.37 min.

ethyl 2-imino-10-methyl-5-oxo-1-(2-(thiophen-2-yl)ethyl)-1,5-dihydro-2H-dipyrido[1,2-a:2',3'-d]pyrimidine-3-carboxylate (7f). Yellow solid (165 mg, 81% yield). ^{1}H NMR (400 MHz, $CDCl_3$) δ 9.57 (s, 1H), 8.86 (d, *J* = 7.1 Hz, 1H), 8.66 (s, 1H), 7.67 (d, *J* = 6.9 Hz, 1H), 7.14 (dd, *J* = 4.9, 1.3 Hz, 1H), 7.02 (t, *J* = 7.0 Hz, 1H), 6.98 – 6.92 (m, 2H), 4.87 – 4.74 (m, 2H), 4.37 (q, *J* = 7.1 Hz, 2H), 3.38 – 3.25 (m, 2H), 2.58 (d, *J* = 18.6 Hz, 3H), 1.42 (t, *J* = 7.1 Hz, 3H). ^{13}C NMR (151 MHz, $CDCl_3$) δ 171.1, 1654, 156.1, 155.7, 154.1, 150.8, 141.4, 137.3, 134.2, 126.8, 126.0, 125.3, 123.5, 114.1, 113.7, 94.5, 61.0, 60.3, 58.3, 43.6, 26.8, 20.9, 18.3, 18.1, 14.2, 14.1. LRMS m/z 409.1 $[M + H]^+$. HPLC purity 96.8%, t_r = 2.23 min.

ethyl 1-(furan-2-ylmethyl)-2-imino-10-methyl-5-oxo-1,5-dihydro-2H-dipyrido[1,2-a:2',3'-d]pyrimidine-3-carboxylate (7g). Yellow solid (158 mg, 84% yield). ^{1}H NMR

(400 MHz, $CDCl_3$) δ 10.31 (s, 1H), 9.28 (s, 1H), 9.03 (d, *J* = 7.1 Hz, 1H), 8.00 (d, *J* = 7.0 Hz, 1H), 7.36 (t, *J* = 7.0 Hz, 1H), 7.25 (s, 1H), 6.99 (d, *J* = 3.2 Hz, 1H), 6.51 (s, 2H), 6.40 – 6.30 (m, 1H), 4.46 (q, *J* = 7.1 Hz, 2H), 2.73 (s, 3H), 1.45 (t, *J* = 7.1 Hz, 3H). ^{13}C NMR (101 MHz, $CDCl_3$) δ 164.2, 156.3, 156.1, 145.9, 144.1, 143.0, 140.5, 137.5, 136.0, 126.6, 116.9, 112.6, 110.8, 99.4, 63.0, 40.9, 18.3, 14.2. LRMS m/z 379.1 $[M + H]^+$. HPLC purity 99.0%, t_r = 2.05 min.

ethyl 1-benzyl-2-imino-10-methyl-5-oxo-1,5-dihydro-2H-dipyrido[1,2-a:2',3'-d]pyrimidine-3-carboxylate (7h). Yellow solid (165 mg, 85% yield). ^1H NMR (400 MHz, $CDCl_3$) δ 9.64 (s, 1H), 8.87 (d, *J* = 7.0 Hz, 1H), 8.71 (s, 1H), 7.63 (d, *J* = 6.6 Hz, 1H), 7.46 (d, *J* = 7.3 Hz, 2H), 7.33 – 7.26 (m, 3H), 7.23 (d, *J* = 7.2 Hz, 1H), 7.01 (t, *J* = 7.0 Hz, 1H), 5.83 (s, 2H), 4.37 (q, *J* = 7.1 Hz, 2H), 2.49 (s, 3H), 1.42 (t, *J* = 7.1 Hz, 3H). ^{13}C NMR (126 MHz, $CDCl_3$) δ 165.0, 156.0, 155.8, 154.0, 150.4, 137.5, 137.1, 136.9, 134.0, 127.8, 127.3, 126.4, 125.7, 113.8, 113.6, 94.3, 60.7, 44.7, 17.8, 13.9. LRMS m/z 389.0 $[M + H]^+$. HPLC purity 100%, t_r = 2.17 min.

ethyl 2-imino-10-methyl-5-oxo-1-phenyl-1,5-dihydro-2H-dipyrido[1,2-a:2',3'-d]pyrimidine-3-carboxylate (7i). Yellow solid (166 mg, 89% yield). ^1H NMR (400 MHz, $CDCl_3$) δ 9.46 (s, 1H), 8.86 (d, *J* = 7.1 Hz, 1H), 8.77 (s, 1H), 7.57 (t, *J* = 7.8 Hz, 3H), 7.47 (t, *J* = 7.4 Hz, 1H), 7.29 (s, 1H), 7.27 (s, 1H), 6.99 (t, *J* = 7.0 Hz, 1H), 4.38 (q, *J* = 7.1 Hz, 2H), 2.04 (s, 3H), 1.43 (t, *J* = 7.1 Hz, 3H). ^{13}C NMR (126 MHz, $CDCl_3$) δ 164.8, 157.4, 155.8, 155.0, 150.2, 138.0, 137.5, 136.7, 134.2, 128.9, 128.3, 127.6, 125.5, 114.3, 113.9, 94.4, 60.7, 16.7, 13.9. LRMS m/z 375.1 $[M + H]^+$. HPLC purity 98.0%, t_r = 1.97 min.

ethyl 1-(4-fluorophenyl)-2-imino-10-methyl-5-oxo-1,5-dihydro-2H-dipyrido[1,2-a:2',3'-d]pyrimidine-3-carboxylate (7j). Yellow solid (176 mg, 90% yield). ^{1}H NMR (400 MHz, $CDCl_3$) δ 8.87 (d, *J* = 7.0 Hz, 1H), 8.77 (s, 1H), 7.59 (d, *J* = 6.8 Hz, 1H), 7.26 (d, *J* = 6.6 Hz, 4H), 7.02 (t, *J* = 7.0 Hz, 1H), 4.39 (q, *J* = 7.1 Hz, 2H), 2.08 (s, 3H), 1.43 (t, *J* = 7.1 Hz, 3H). ^{13}C NMR (126 MHz, $CDCl_3$) δ 164.7, 162.6, 160.7, 157.4, 155.7, 154.9, 150.3, 137.7, 137.1, 134.2, 133.6, 130.1, 129.8, 125.6, 116.1, 115.9, 114.1, 94.6, 60.8, 16.8, 13.9. LRMS m/z 393.1 $[M + H]^+$. HPLC purity 99.0%, t_r = 1.99 min.

General synthetic procedure for compound 8. To a solution of compound **7** (0.15 mmol, 1.0 eq) in THF/EtOH (6 mL, 1/2 vol/vol) was added a solution of LiOH (18 mg, 0.75 mmol, 5.0 eq) in water (1 mL) at rt. The mixture was stirred at 40 °C overnight. After the complete consumption of compound **7** monitored in TLC, the mixture was condensed under vacuum. Then, the residue was dissolved in H_2O. After the solution was adjusted to pH 4.0, a light-yellow solid appeared. A simple filtration provided compound **8** as a solid.

2-imino-1-isopropyl-10-methyl-5-oxo-1,5-dihydro-2H-dipyrido[1,2-a:2',3'-d]pyrimidine-3-carboxylic acid (8a). Yellow solid (41 mg, 88% yield). ^{1}H NMR (400 MHz, DMSO-d_6) δ 14.48 (s, 1H), 8.91 (d, *J* = 10.3 Hz, 2H), 8.05 (d, *J* = 6.1 Hz, 1H), 7.37 (t, *J* = 7.0 Hz, 1H), 2.60 (s, 3H), 1.77 (d, 6H). ^{13}C NMR (126 MHz, DMSO-d_6) δ 164.4, 156.7, 149.0, 139.1, 138.9, 133.6, 126.1, 117.8, 116.0, 100.0, 17.9. HPLC purity 100%, t_r = 1.46 min.

2-imino-10-methyl-5-oxo-1-propyl-1,5-dihydro-2H-dipyrido[1,2-a:2',3'-d]pyrimidine-3-carboxylic acid (8b). Yellow solid (40 mg, 86% yield). ^{1}H NMR (500 MHz, TFA-*d*) δ 9.64 (s, 1H), 9.13 (d, *J* = 6.7 Hz, 2H), 8.16 (d, *J* = 6.7 Hz, 2H), 7.49 (t, *J* = 6.9 Hz, 1H), 4.82 (s, 3H), 2.78 (s, 3H), 2.04 (d, *J* = 7.4 Hz, 3H), 1.20 (t, *J* = 7.0 Hz, 3H). ^{13}C NMR (126 MHz, TFA-*d*) δ 159.1, 148.9, 147.0, 142.1, 137.6, 132.7, 126.9, 117.1, 108.7, 106.4, 105.5, 104.1, 103.3, 96.6, 91.2, 37.2, 9.5. HPLC purity 100%, t_r = 1.48 min.

2-imino-10-methyl-5-oxo-1-phenethyl-1,5-dihydro-2H-dipyrido[1,2-a:2',3'-d]pyrimidine-3-carboxylic acid (8c). Yellow solid (47 mg, 83% yield). ^{1}H NMR (400 MHz, TFA-*d*) δ 11.65 (s, 1H), 9.95 (s, 1H), 9.00 (s, 1H), 8.96 (d, *J* = 7.0 Hz, 1H), 8.16 (d, *J* = 6.8 Hz, 1H), 7.46 (t, *J* = 7.1 Hz, 1H), 7.39 (d, *J* = 7.6 Hz, 2H), 7.31 (t, *J* = 7.4 Hz, 2H), 7.21 (t, *J* = 7.3 Hz, 1H), 4.91 (s, 2H), 3.07 (t, *J* = 7.6 Hz, 3H), 2.57 (s, 3H). ^{13}C NMR (126 MHz, TFA-*d*) δ 165.7, 156.5, 150.6, 150.3, 141.8, 140.6, 137.3, 133.9, 129.0, 128.4, 126.7, 116.8, 99.7, 44.8, 31.5, 17.4. HPLC purity 96.2%, t_r = 1.59 min. LRMS m/z 375.2 $[M + H]^+$. HPLC purity 95.8%, t_r = 1.57 min.

1-(4-chlorophenethyl)-2-imino-10-methyl-5-oxo-1,5-dihydro-2H-dipyrido[1,2-a:2',3'-d]pyrimidine-3-carboxylic acid (8d). Yellow solid (52 mg, 84% yield). ^{1}H NMR (400 MHz, TFA-*d*) δ 9.62 (s, 1H), 9.10 (d, *J* = 6.8 Hz, 1H), 8.15 (d, *J* = 7.0 Hz, 1H), 7.48 (t, *J* = 7.0 Hz, 1H), 7.18 (q, *J* = 8.3 Hz, 5H), 5.16 (s, 2H), 3.30 (t, *J* = 6.5 Hz, 2H), 2.74 (s, 3H). ^{13}C NMR (126 MHz, TFA-*d*) δ 164.3, 154.0, 147.4, 147.2, 142.9, 138.1, 131.9, 129.9, 129.6, 125.4, 124.6, 122.5, 101.8, 96.3, 41.6, 26.8, 12.3. LRMS m/z 409.2 $[M + H]^+$.

2-imino-10-methyl-1-(4-methylphenethyl)-5-oxo-1,5-dihydro-2H-dipyrido[1,2-a:2',3'-d]pyrimidine-3-carboxylic acid (8e). Yellow solid (50 mg, 85% yield). ^{1}H NMR (400 MHz, TFA-*d*) δ 9.57 (s, 1H), 9.05 (d, *J* = 6.8 Hz, 1H), 8.10 (d, *J* = 6.8 Hz, 1H), 7.43 (t, *J* = 6.8 Hz, 1H), 7.01 (s, 5H), 5.06 (s, 2H), 3.24 (s, 2H), 2.72 (s, 3H), 2.15 (s, 3H). ^{13}C NMR (126 MHz, TFA-*d*) δ 164.3, 154.0, 152.5, 147.4, 147.2, 142.9, 137.9, 134.0, 132.1, 128.3, 125.3, 123.8, 122.3, 114.0, 101.7, 96.4, 42.4, 27.2, 14.7, 12.3. LRMS m/z 389.1 $[M + H]^+$.

2-imino-10-methyl-5-oxo-1-(2-(thiophen-2-yl)ethyl)-1,5-dihydro-2H-dipyrido[1,2-a:2',3'-d]pyrimidine-3-carboxylic acid (8f). Yellow solid (50 mg, 88% yield). ^{1}H NMR (400 MHz, TFA-*d*) δ 9.60 (s, 1H), 9.09 (d, *J* = 6.9 Hz, 1H), 8.12 (d, *J* = 6.7 Hz, 1H), 7.46 (t, *J* = 7.0 Hz, 1H), 6.85 (s, 1H), 5.11 (s, 2H), 3.55 (d, *J* = 6.0 Hz, 2H), 2.75 (s, 3H). ^{13}C NMR (126 MHz, TFA-*d*) δ 164.3, 154.0, 152.7, 147.4, 143.1, 138.1, 132.7, 132.2, 122.9, 122.4, 114.1, 101.7, 96.4, 42.4, 21.7, 12.4. LRMS m/z 381.1 $[M + H]^+$. HPLC purity 95.4%, t_r = 1.49 min.

1-(furan-2-ylmethyl)-2-imino-10-methyl-5-oxo-1,5-dihydro-2H-dipyrido[1,2-a:2',3'-d]pyrimidine-3-carboxylic acid (8g). Yellow solid (44 mg, 83% yield). ^{1}H NMR (400 MHz, TFA-*d*) δ 9.58 (s, 1H), 9.10 (d, *J* = 6.8 Hz, 1H), 8.16 (d, *J* = 6.7 Hz, 1H), 7.45 (dd, *J* = 25.8, 18.7 Hz, 2H), 7.38 (s, 1H), 6.68 (d, *J* = 2.6 Hz, 1H), 6.39 (s, 1H), 6.04 (s, 2H), 2.81 (s, 3H). ^{13}C NMR (126 MHz, TFA-*d*) δ 164.3, 153.9, 153.1, 147.2, 144.0, 143.1, 140.6, 140.2, 139.7, 138.3, 132.1, 128.9, 123.4, 122.5, 114.1, 101.9, 96.4, 36.9, 12.2, 11.6. LRMS m/z 351.1 $[M + H]^+$.

General synthetic procedure for compound 10. A mixture of aldehyde **9** (1.2 g, 10 mmol) and diethyl malonate (2.4 g, 15 mmol) was stirred for 24 hr in the presence of a catalytic amount of piperidine. After the completion of the reaction, ethyl acetate was added to the mixture. Then, a simple filtration provided compound **10** as a yellow solid, which was directly subjected to the next step without further purification.

General synthetic procedure for compound 11. Compound **10** (3 mmol) and K_2CO_3 (6 mmol) were dissolved in DMF (15 mL) at rt and then alkyl halide (4.5 mmol) was added. The resulting mixture was stirred at rt overnight. After completion of the reaction, compound **11** was purified by silica-chromatography as a white solid.

ethyl 2-oxo-1-phenethyl-1,2-dihydro-1,8-naphthyridine-3-carboxylate (11a). White solid (41 mg, 64% yield). ^{1}H NMR (400 MHz, $CDCl_3$) δ 8.73 (dd, *J* = 4.7, 1.7 Hz, 1H), 8.40 (s, 1H), 8.00 (dd, *J* = 7.7, 1.6 Hz, 1H), 7.43 (d, *J* = 7.3 Hz, 2H), 7.34 (t, *J* = 7.5 Hz, 2H), 7.25 (dd, *J* = 7.7, 4.7 Hz, 2H), 4.83 – 4.72 (m, 2H), 4.47 (q, *J* = 7.1 Hz, 2H), 3.09 – 2.99 (m, 2H), 1.46 (t, *J* = 7.1 Hz, 3H). ^{13}C NMR (151 MHz, $CDCl_3$) δ 164.6, 159.3, 152.4, 150.4, 141.8, 139.0, 138.0, 129.1, 128.5, 126.4, 124.3, 118.5, 114.1, 61.8, 43.2, 33.9, 14.4. LRMS m/z 323.0 $[M + H]^+$. HPLC purity 95.8%, t_r = 2.05 min.

ethyl 2-oxo-1-phenethyl-1,2-dihydro-1,6-naphthyridine-3-carboxylate (11b). White solid (51 mg, 79% yield). ^{1}H NMR (500 MHz, $CDCl_3$) δ 8.89 (s, 1H), 8.63 (d, *J* = 6.1 Hz, 1H), 8.49 (s, 1H), 7.36 – 7.30 (m, 4H), 7.28 – 7.24 (m, 1H), 7.14 (d, *J* = 6.1 Hz, 1H), 4.50 – 4.39 (m, 4H), 3.08 – 3.01 (m, 2H), 1.46 (t, *J* = 7.1 Hz, 3H). ^{13}C NMR (126 MHz,

$CDCl_3$) δ 164.0, 158.5, 152.3, 151.5, 145.3, 141.8, 137.6, 128.8, 127.0, 124.2, 115.2, 108.1, 61.9, 44.5, 33.5, 14.3. LRMS m/z 323.0 $[M + H]^+$. HPLC purity 95.4%, t_r = 1.87 min.

General synthetic procedure for compound 12. To a solution of compound **11** (1.5 mmol, 1.0 eq) in THF/EtOH (18 mL, 1/2 vol/vol) was added a solution of LiOH (7.5 mmol, 5.0 eq) in water (3 mL) at rt. The mixture was stirred at 40 °C overnight. After complete consumption of compound **11** monitored by TLC, the mixture was condensed under vacuum, and the residue was dissolved in H_2O. After the pH was adjusted to 4.0, a light-yellow solid appeared. After filtration, compound **12** was obtained as white solid.

2-oxo-1-phenethyl-1,2-dihydro-1,8-naphthyridine-3-carboxylic acid (12a). White solid (36 mg, 61% yield). ^{1}H NMR (400 MHz, DMSO-d_6) δ 14.21 (s, 1H), 8.98 (s, 1H), 8.89 (dd, *J* = 4.7, 1.8 Hz, 1H), 8.56 (dd, *J* = 7.8, 1.8 Hz, 1H), 7.54 (dd, *J* = 7.8, 4.7 Hz, 1H), 7.35 – 7.26 (m, 4H), 7.26 – 7.18 (m, 1H), 4.86 – 4.63 (m, 2H), 3.10 – 2.86 (m, 2H). ^{13}C NMR (126 MHz, DMSO-d_6) δ 164.6, 163.6, 154.0, 149.5, 144.6, 140.5, 138.8, 129.1, 128.9, 126.9, 120.6, 119.9, 115.4, 43.1, 33.6. LRMS m/z 295.1 $[M + H]^+$. HPLC purity 100%, t_r = 1.57 min.

2-oxo-1-phenethyl-1,2-dihydro-1,6-naphthyridine-3-carboxylic acid (12b). White solid (43 mg, 73% yield). ^{1}H NMR (400 MHz, DMSO-d_6) δ 14.22 (s, 1H), 8.98 (s, 1H), 8.89 (dd, *J* = 4.6, 1.8 Hz, 1H), 8.56 (dd, *J* = 7.8, 1.8 Hz, 1H), 7.54 (dd, *J* = 7.8, 4.7 Hz, 1H), 7.35 – 7.26 (m, 4H), 7.26 – 7.19 (m, 1H), 4.73 (dd, *J* = 9.1, 6.8 Hz, 2H), 3.12 – 2.86

(m, 2H). ^{13}C NMR (126 MHz, DMSO-d_6) δ 164.6, 163.6, 154.0, 149.5, 144.6, 140.5, 138.8, 129.1, 128.9, 126.9, 120.6, 119.9, 115.4, 43.1, 33.6. LRMS m/z 295.1 $[M + H]^+$. HPLC purity 100%, t_r = 1.58 min.

General synthetic procedure for compounds 13 and 14. A mixture of compound **12** (0.2 mmol, 1.0 eq) and HATU (0.3 mmol, 1.5 eq) in DMF (4 mL) was stirred at rt for 5 min, then DIEA (0.6 mmol, 3.0 eq) and the corresponding amine (0.3 mmol, 1.5 eq) was added. The resulting solution was stirred at rt overnight. After the completion of the reaction, white precipitate appeared by the addition of an identical amount of water. Target compounds **13** and **14** were obtained by a simple filtration.

N-(4-fluorophenethyl)-2-oxo-1-phenethyl-1,2-dihydro-1,8-naphthyridine-3-carboxamide (13a). White solid (48 mg, 58% yield). ^{1}H NMR (400 MHz, DMSO-d_6) δ 9.71 (t, *J* = 5.7 Hz, 1H), 8.90 (s, 1H), 8.82 (d, *J* = 4.7 Hz, 1H), 8.51 (d, *J* = 7.7 Hz, 1H), 7.46 (dd, *J* = 7.8, 4.7 Hz, 1H), 7.35 – 7.26 (m, 3H), 7.23 (t, *J* = 7.0 Hz, 1H), 7.14 (t, *J* = 8.8 Hz, 1H), 4.75 – 4.63 (m, 2H), 3.60 (dd, *J* = 13.5, 6.8 Hz, 2H), 2.99 – 2.90 (m, 2H), 2.87 (t, *J* = 7.4 Hz, 2H). ^{13}C NMR (151 MHz, DMSO-d_6) δ 162.6, 162.1, 160.6, 153.0, 149.5, 142.5, 139.9, 139.1, 135.9, 131.0, 129.1, 129.0, 126.9, 122.7, 119.9, 115.6, 115.5, 115.0, 42.8, 41.0, 34.7, 33.8. LRMS m/z 404.2 $[M + H]^+$. HPLC purity 100%, t_r = 2.22 min.

N-(2-(diethylamino)ethyl)-2-oxo-1-phenethyl-1,2-dihydro-1,8-naphthyridine-3-carboxamide (13b). White solid (46 mg, 59% yield). ^{1}H NMR (400 MHz, DMSO-d_6) δ 9.74 (t, *J* = 5.4 Hz, 1H), 8.91 (s, 1H), 8.81 (dd, *J* = 4.6, 1.7 Hz, 1H), 8.50 (dd, *J* = 7.8, 1.7

Hz, 1H), 7.45 (dd, *J* = 7.8, 4.7 Hz, 1H), 7.35 – 7.26 (m, 4H), 7.22 (t, *J* = 6.8 Hz, 1H), 4.86 – 4.63 (m, 2H), 3.42 (q, *J* = 6.2 Hz, 2H), 3.03 – 2.85 (m, 2H), 2.63 – 2.51 (m, 7H), 1.00 (t, *J* = 7.1 Hz, 6H). ^{13}C NMR (151 MHz, DMSO-d_6) δ 162.5, 162.0, 152.9, 149.6, 142.4, 139.9, 139.1, 129.1, 128.9, 126.9, 122.9, 119.8, 115.0, 51.7, 47.1, 42.7, 37.9, 33.7. LRMS m/z 393.3 $[M + H]^+$. HPLC purity 100%, t_r = 2.20 min.

N-(4-fluorophenethyl)-2-oxo-1-phenethyl-1,2-dihydro-1,6-naphthyridine-3-carboxamide (14a). White solid (69 mg, 85% yield). ^{1}H NMR (400 MHz, DMSO-d_6) δ 9.57 (s, 1H), 9.16 (s, 1H), 8.94 (s, 1H), 8.66 (d, *J* = 6.0 Hz, 1H), 7.65 (d, *J* = 6.1 Hz, 1H), 7.32 (s, 6H), 7.24 (d, *J* = 5.9 Hz, 1H), 7.13 (t, *J* = 8.8 Hz, 2H), 4.54 – 4.41 (m, 2H), 3.59 (dd, *J* = 13.4, 6.8 Hz, 2H), 2.99 – 2.90 (m, 2H), 2.86 (t, *J* = 7.2 Hz, 2H). ^{13}C NMR (126 MHz, DMSO-d_6) δ 162.4, 161.0, 160.4, 153.3, 151.6, 144.5, 142.2, 138.4, 135.9, 130.9, 129.4, 128.9, 127.1, 123.1, 115.8, 115.6, 115.4, 109.7, 44.1, 41.00, 34.7, 33.3. LRMS m/z 416.1 $[M + H]^+$. HPLC purity 97.5%, t_r = 2.07 min.

N-(2-(diethylamino)ethyl)-2-oxo-1-phenethyl-1,2-dihydro-1,6-naphthyridine-3-carboxamide (14b). White solid (71 mg, 90% yield). ^{1}H NMR (400 MHz, DMSO-d_6) δ 9.61 (t, *J* = 5.3 Hz, 1H), 9.16 (s, 1H), 8.95 (s, 1H), 8.65 (d, *J* = 6.1 Hz, 1H), 7.64 (d, *J* = 6.2 Hz, 1H), 7.37 – 7.27 (m, 4H), 7.22 (dd, *J* = 7.9, 4.9 Hz, 1H), 4.57 – 4.44 (m, 2H), 3.47 – 3.37 (m, 2H), 2.99 – 2.90 (m, 2H), 2.56 (dd, *J* = 13.5, 6.8 Hz, 4H), 0.99 (t, *J* = 7.1 Hz, 6H). ^{13}C NMR (126 MHz, DMSO-d_6) δ 162.3, 161.7, 153.2, 151.5, 144.5, 142.1, 138.4, 129.3, 128.9, 127.0, 123.2, 115.8, 109.7, 51.7, 47.1, 44.0, 37.9, 33.3, 12.4. LRMS m/z 393.2 $[M + H]^+$. HPLC purity 98.8%, t_r = 1.83 min.

Proteins expression and purification. The DNA sequence encoding $SPOP^{MATH}$ were subcloned into the *BamHI* and *XhoI* restriction sites of the modified pGEX-6P-1 with dual tags of GST and His at *N*-terminus. The DNA sequence encoding SPOP (residue 23-337 or full-length) was cloned into the *BamHI* and *XhoI* restriction sites of the modified pET-23a. The *Escherichia coli* BL21 (DE3) strain was transformed with the recombinant plasmids and grown in lysogeny broth (LB) at 37 °C in the presence of 100 μg/mL ampicillin. When the A_{600} reached 0.6-0.8, protein expression was induced by IPTG with a final concentration of 0.5 mM for an additional 16-18 hr at 16 °C. The cells were harvested by centrifugation at 5,000 g for 10 min and stored at -80 °C.

For protein purification, the cells were suspended in 40 mL lysis buffer (20 mM Tris-HCl (pH 7.5), 150 mM NaCl, 1 mM DTT), lysed by sonification, and centrifuged at 12,000 g for 25 min at 4 °C. The supernatant was passed through 0.45 μm syringe filters and loaded onto HisTrap HP column (5 mL, GE Healthcare), washed with seven column volumes of 30 mM imidazole, and finally eluted with 300 mM imidazole. Proteins were concentrated via centrifugal filtration with a cutoff of 10 kDa molecular weight. Further purification was conducted through gel filtration (HiLoad 16/60 Superdex 200, GE Healthcare). Fractions were collected and checked by 12% SDS-PAGE. SPOP protein was stored at -80 °C.

Nano Differential Scanning Fluorimetry (nanoDSF) assay. To a solution of 1 mg/mL of $SPOP^{MATH}$ protein in buffer (150 mM NaCl, 100 mM sodium citrate, pH 5.1) or 1 mg/mL of $SPOP^{23-337}$ protein in buffer (150 mM NaCl, 20 mM Tris-HCl, pH 7.5) were

added a solution of 0.5 μL compound in DMSO to the appropriate concentration. After incubation for 15 min at rt, the mixture was centrifuged for 2 min at 1,000 g in order to remove any precipitates. Approximately 10 μL of the supernatant fraction was loaded to each capillary, and which was then placed on the holder in the sample rack. The thermal denaturation curves were determined by the measurement of the protein intrinsic fluorescence on label-free native nanoDSF (NanoTemper, Prometheus NT.48). The temperature was increased from 20 °C to 90 °C at a rate of 2 deg·min^{-1}. Tryptophan residues in SPOP were excited at 280 nm and the fluorescence intensity was recorded at 330 nm and 350 nm, respectively.

Conventional DSF assay. The conventional DSF assay was performed on the Bio-Rad 96 system (Bio-Red, CFx 96 Touch) using SYPRO orange (Invitrogen) as a dye. The mixture containing 10 μM SPOP^{MATH}, 5× SYPRO dye, and different concentrations of compound were heated from 25 °C to 95 °C at a 1% ramp rate on Bio-Rad 96 system (Bio-Red, CFx 96 Touch). The fluorescence intensity was detected at the wavelength of 492 nm for excitation and 610 nm for emission. The melting temperature (Tm) of protein was calculated by Bio-Rad CFx Manager 3.1 (Bio-Rad) and was further normalized by Origen 8.0.

Nuclear Magnetic Resonance (NMR) titration. Phosphate buffer (PBS) containing 20 mM sodium phosphate (pH 7.4), 100 mM NaCl, 5% DMSO was used for NMR. All NMR spectra were acquired on a Bruker Avance III-600 MHz spectrometer equipped with a cryogenically cooled probe (Bruker biospin, Germany) at 25 °C. Samples

contained 200 μM compound and $SPOP^{MATH}$ or $SPOP^{1-374}$ protein at varying concentrations of 0, 5 μM, 10 μM, and 20 μM or 0, 1 μM, 2 μM, 4 μM, and 8 μM.

Surface Plasmon Resonance (SPR). The SPR assay was run on a Biacore T200 instrument (GE Healthcare). The running buffer was 1× PBS-P^+ (10 mM PBS-P^+ (pH 7.4), 137 mM NaCl, 2.7 mM KCl, 0.5% (v/v) surfactant P20, 5% DMSO). $SPOP^{MATH}$ or $SPOP^{1-374}$ were covalently immobilized onto sensor CM5 chips by a standard amine-coupling procedure in 10 mM of sodium acetate (pH 4.5). A series of compounds were diluted and injected onto a sensor chip at a flow rate of 30 μL/min for 120 sec (contact phase), followed by 120 sec of buffer flow (dissociation phase). The K_D value was derived through the use of Biacore T200 Evaluation software Version 1.0 (GE Healthcare) and steady state analysis of data at equilibrium.

Cell cultures. HEK293T, A498, A549, H1299, U251 and HS766T were purchased from ATCC (Rockville, MD, USA), and maintained in DMEM medium supplemented with 10% FBS (Gibco), 100 units/mL streptomycin, and 100 units/mL penicillin. OS-RC-2 was obtained from the National Platform of Experimental Cell Resources for Sci-Tech (Beijing, China), and maintained in a RPMI1640 medium supplemented with 10% FBS (Gibco), 100 units/mL streptomycin, and 100 units/mL penicillin. The culture medium was changed every two (2) days. Cells for the subculture were detached and harvested by 0.25% trypsin and 0.02% EDTA. All cells were cultured at 37 °C in a humidified, 5% CO_2-containing atmosphere incubator (Thermo Scientific). All cells were regularly checked to be mycoplasma-free.

Cell proliferation assay. Cell proliferation was determined by an MTT assay. A498 and OS-RC-2 cells (1,000 - 2,200/well) were seeded into 96-well plates and cultured at 37 °C for 12 hr, then the compounds were added. After cells were cultured for an additional 72 hr, 10 μL MTT reagent was added to each well. The plates were incubated for 4 hr. The supernatants were then aspirated, and the formazan crystals in each well were dissolved in 150 μL DMSO. Absorbance was measured by microplate reader at a wavelength of 490 nm. The optical density of formazan formed in untreated cells was taken as 100% proliferation. Luminescence was read by Spark 10M (Tecan).

Colony formation assay. A498 and OS-RC-2 ccRCC cells were seeded into each well of a six-well plate at a density of 1,000 cells/well and incubated for 12 days at 37 °C in 5% CO_2. The culture medium was refreshed every three (3) days. The cells were fixed with 10% acetic acid and 10% methanol for 15 min, then stained with 1% crystal violet for 10 min.

Real-Time quantitative PCR (RT-qPCR). A498 and OS-RC-2 cells were treated with multiple doses of **6lc**. Total RNA was extracted with Trizol Reagent Kit (Sigma). And then equivalent amounts of RNA were reversed-transcribed into cDNA using the HiScript III RT SuperMix for qPCR Kit (Vazyme, R323-01). RT-qPCR reactions were performed using the ChamQ Universal SYBR qPCR Master Mix (Vazyme, Q711-02/03) in the CFX96 Touch Real-Time PCR Detection System (Bio-Rad). Gene expression was calculated through the use of the comparative *ΔΔ*CT method with the GAPDH for normalization. The primers used are as follows: DUSP7, tctgactgctccgacggcga

(forward), ccttggcgcagccgaggtag (reverse); PTEN, ttgagccgctgtgaggcgag (forward), agccgaggaagaggctgcac (reverse); GAPDH, cgaccactttgtcaagctca (forward), ccctgttgctgtagccaaat (reverse).

Antibodies. SPOP (Abcam, ab137537), Flag (Sigma, F1804), Myc (Sigma, M4439), HA (Sigma, H9658), GAPDH (Sigma, G8795), PTEN (Cell Signaling, #9559), DUSP7 (ABGENT, AP8450a), AKT (Cell Signaling, #9272), p-AKT (Thr308) (Cell signaling, #4056), ERK1/2 (Cell Signaling, # 9102), and p-ERK1/2 (Thr202/Tyr204) (Cell Signaling, #4376).

Western blot. Cells were treated with SPOP inhibitor at different concentrations for 12 hr. The cells were harvested with RIPA lysis buffer (Beyotime, P0013C), and centrifuged at 14,000 g for 20 min at 4 °C. The supernatants were centrifuged, and protein concentration was quantified with BCA assay (ThermoFisher, 23225). The sample was diluted with 5× loading butter and was heated for 5 min at 100 °C and then analyzed on 12% SDS-PAGE. The proteins in SDS-PAGE were transferred onto nitrocellulose membrane (Millipore, USA), which was blocked with 5% skim milk for 1 hr at rt. The membrane was incubated with primary antibody at 4 °C overnight. HRP-labeled Goat Anti-mouse or Anti-rabbit IgG was used as a secondary antibody. The membrane was visualized using the ECL detection system (GE Healthcare Bioscience, USA). Equivalent amounts of total protein were monitored by GAPDH as loading control.

Co-immunoprecipitation (Co-IP). HEK293T cells were transiently transfected with the indicated plasmids, SPOP-p3×Flag-CMV10 and PTEN-pcDNA4-myc-His, respectively. After 36 hr transfection, cells were treated with SPOP inhibitor at different concentrations for 12 hr. The cells were harvested with lysis buffer (50 mM Tris-HCl (pH 7.5), 150 mM NaCl, 1% Triton x 100, 1 mM EDTA, 1 mM NaF, 1 mM Na_3VO_4, and 1× proteinase inhibitor cocktail (Sigma, P8340)), and centrifuged at 14,000 g for 20 min at 4 °C. Supernatants were centrifuged and protein concentration was quantified with BCA assay (ThermoFisher, 23225). For immunoprecipitation, the supernatants were immunoprecipitated with anti-Myc-conjugated agarose beads (Sigma, rabbit antibody) for 2 hr at 4 °C. Then the beads were washed 7 times with lysis buffer, and then the sample was diluted with 5× loading buffer. Heat the samples for 5 min at 100 °C and then subjected to western blot analysis. For whole cell lysates, supernatants were diluted with 5× loading buffer, heated for 5 min at 100 °C, and then subjected to western blot analysis.

Ubiquitination assay. HEK293T cells were transfected in 60 mm dishes with 1 μg each of Myc-PTEN, Flag-SPOP-cyto, and HA-Ub. After 36 hr culture, cells were treated with **6lc** for 8 hr, and then cells were treated with 10 μM MG132 (Calbiochem) for another 4 hr before harvesting. Cells were harvested in a denaturing buffer (1% SDS, 50 mM Tris-HCl (pH 7.5), 0.5 mM EDTA, 1 mM DTT). The lysate was incubated for 5 min at 100 °C immediately, and then sonicated and diluted ten times with RIPA lysis buffer. For immunoprecipitation, the lysates were subjected to co-immunoprecipitation using anti-Myc-conjugated agarose beads as

described in Co-IP assay. For whole cell lysates, the lysates were diluted with 5× loading buffer, heated for 5 min at 100 °C, and then subjected to western blot analysis.

Drug Affinity Responsive Target Stability (DARTS) assay. The DARTS assay was performed on the basis of the reported protocol. [22] Briefly, 1×10^6 A498 or OS-RC-2 cells were collected and washed with ice-cold PBS. Then, cells were lysed with lysis buffer in M-PER reagent (ThermoFisher, 78501) with a protease inhibitor cocktail (ThermoFisher, 78430) and phosphatase inhibitor cocktail (ThermoFisher, 78420). Cell lysis was incubated on ice for 10 min and centrifuged for 10 min at 18,000 g at 4 °C. The supernatant was removed and transferred into TNC buffer (50 mM Tris-HCl (pH 8.0), 50 mM NaCl and 10 mM $CaCl_2$). Protein concentration was quantified with BCA assay (ThermoFisher, 23225). Cell suspension was distributed into different 1.5 mL PCR tubes (120 μg), incubated with diffident concentrations of compound (0, 1 μM, 5 μM, 10 μM, and 50 μM) for 20 min at rt, and then subsequently digested with pronase (1:1000 for A498 and 1:2000 for OS-RC-2) for 10 min at rt. The reaction was stopped by adding a protease inhibitor cocktail for 10 min on ice. Finally, the supernatants were diluted with 5× loading buffer, heated for 5 min at 70 °C, and then subjected to western blot analysis.

ASSOCIATED CONTENT

Supporting Information

The Supporting Information is available free of charge on the ACS Publications website at DOI:

Additional tables and figures illustrating properties of SPOP inhibitors, synthetic methods and analytical data for target compounds (PDF)

Molecular formula strings and biological data (CSV)

AUTHOR INFORMATION

Corresponding Author

*yangcg@simm.ac.cn

Author Contributions

§ Z.D. and Z.W. contributed equally.

Notes

The authors declare no competing financial interest.

ACKNOWLEDGEMENTS

This work was supported in part by grants from the National Natural Science Foundation of China (21807103 to Z.D. and 21725801 to C.-G.Y.), the National Science & Technology Major Project “Key New Drug Creation and Manufacturing Program”, China (2018ZX09711002 to Z.D.). We thank S.F. Reichard, MA for editing the manuscript.

ABBREVIATIONS

ccRCC, clear-cell renal cell carcinomas; CMPG, Carr-Purcell-Meiboom-Gill; Co-IP, Co-immunoprecipitation; DARTS, drug affinity responsive target stability; DUSP7, dual-specificity phosphatase 7; mTOR, mammalian target of rapamycin; nanoDSF, nano differential scanning fluorimetry; PAINS, pan assay interference compound; PDGF, platelet-derived growth factor; PTEN, phosphatase-and-tensin homolog; RCC, renal cell carcinomas; RT-qPCR, Real-time quantitative PCR; SPOP, Speckle-type POZ protein; SPR, surface plasmon resonance; STD, saturation transfer difference.

REFERENCES

(1) Ricketts, C. J.; Crooks, D. R.; Linehan, W. M. Targeting HIF2α in clear-cell renal cell carcinoma. *Cancer Cell* **2016**, 30, 515-517.

(2) Rini, B. I.; Campbell, S. C.; Escudier, B. Renal cell carcinoma. *The Lancet* **2009**, 373, 1119-1132.

(3) Presta, L. G.; Chen, H.; O'Connor, S. J.; Chisholm, V.; Meng, Y. G.; Krummen, L.; Winkler, M.; Ferrara, N. Humanization of an anti-vascular endothelial growth factor monoclonal antibody for the therapy of solid tumors and other disorders. *Cancer Res.* **1997**, 57, 4593-4599.

(4) Chen, W.; Hill, H.; Christie, A.; Kim, M. S.; Holloman, E.; Pavia-Jimenez, A.; Homayoun, F.; Ma, Y.; Patel, N.; Yell, P.; Hao, G.; Yousuf, Q.; Joyce, A.; Pedrosa, I.; Geiger, H.; Zhang, H.; Chang, J.; Gardner, K. H.; Bruick, R. K.; Reeves, C.; Hwang, T. H.; Courtney, K.; Frenkel, E.; Sun, X.; Zojwalla, N.; Wong, T.; Rizzi, J. P.; Wallace, E. M.; Josey, J. A.; Xie, Y.; Xie, X. J.; Kapur, P.; McKay, R. M.; Brugarolas, J. Targeting renal cell

carcinoma with a HIF-2 antagonist. *Nature* **2016**, 539, 112-117.

(5) Cho, H.; Du, X.; Rizzi, J. P.; Liberzon, E.; Chakraborty, A. A.; Gao, W.; Carvo, I.; Signoretti, S.; Bruick, R. K.; Josey, J. A.; Wallace, E. M.; Kaelin, W. G. On-target efficacy of a HIF-2α antagonist in preclinical kidney cancer models. *Nature* **2016**, 539, 107-111.

(6) Cuneo, M. J.; Mittag, T. The ubiquitin ligase adaptor SPOP in cancer. *FEBS J.* **2019**, 286, 3946-3958.

(7) Wei, X.; Fried, J.; Li, Y.; Hu, L.; Gao, M.; Zhang, S.; Xu, B. Functional roles of speckle-type Poz (SPOP) Protein in Genomic stability. *J. Cancer* **2018**, 9, 3257-3262.

(8) Mani, R.-S. The emerging role of speckle-type POZ protein (SPOP) in cancer development. *Drug Discovery Today* **2014**, 19, 1498-1502.

(9) Kwon, J. E.; La, M.; Oh, K. H.; Oh, Y. M.; Kim, G. R.; Seol, J. H.; Baek, S. H.; Chiba, T.; Tanaka, K.; Bang, O. S.; Joe, C. O.; Chung, C. H. BTB domain-containing speckle-type POZ protein (SPOP) serves as an adaptor of Daxx for ubiquitination by Cul3-based ubiquitin ligase. *J. Biol. Chem.* **2006**, 281, 12664-12672.

(10) Errington, W. J.; Khan, M. Q.; Bueler, S. A.; Rubinstein, J. L.; Chakrabartty, A.; Prive, G. G. Adaptor protein self-assembly drives the control of a cullin-RING ubiquitin ligase. *Structure* **2012**, 20, 1141-1153.

(11) Zhuang, M.; Calabrese, M. F.; Liu, J.; Waddell, M. B.; Nourse, A.; Hammel, M.; Miller, D. J.; Walden, H.; Duda, D. M.; Seyedin, S. N.; Hoggard, T.; Harper, J. W.; White, K. P.; Schulman, B. A. Structures of SPOP-substrate complexes: insights into molecular architectures of BTB-Cul3 ubiquitin ligases. *Mol. Cell* **2009**, 36, 39-50.

(12) Liu, J.; Ghanim, M.; Xue, L.; Brown, C. D.; Iossifov, I.; Angeletti, C.; Hua, S.; Negre,

N.; Ludwig, M.; Stricker, T.; Al-Ahmadie, H. A.; Tretiakova, M.; Camp, R. L.; Perera-Alberto, M.; Rimm, D. L.; Xu, T.; Rzhetsky, A.; White, K. P. Analysis of Drosophila segmentation network identifies a JNK pathway factor overexpressed in kidney cancer. *Science* **2009**, 323, 1218-1222.

(13) Li, G.; Ci, W.; Karmakar, S.; Chen, K.; Dhar, R.; Fan, Z.; Guo, Z.; Zhang, J.; Ke, Y.; Wang, L.; Zhuang, M.; Hu, S.; Li, X.; Zhou, L.; Li, X.; Calabrese, M. F.; Watson, E. R.; Prasad, S. M.; Rinker-Schaeffer, C.; Eggener, S. E.; Stricker, T.; Tian, Y.; Schulman, B. A.; Liu, J.; White, K. P. SPOP promotes tumorigenesis by acting as a key regulatory hub in kidney cancer. *Cancer Cell* **2014**, 25, 455-468.

(14) Guo, Z. Q.; Zheng, T.; Chen, B.; Luo, C.; Ouyang, S.; Gong, S.; Li, J.; Mao, L. L.; Lian, F.; Yang, Y.; Huang, Y.; Li, L.; Lu, J.; Zhang, B.; Zhou, L.; Ding, H.; Gao, Z.; Zhou, L.; Li, G.; Zhou, R.; Chen, K.; Liu, J.; Wen, Y.; Gong, L.; Ke, Y.; Yang, S. D.; Qiu, X. B.; Zhang, N.; Ren, J.; Zhong, D.; Yang, C. G.; Liu, J.; Jiang, H. Small-molecule targeting of E3 ligase adaptor SPOP in kidney cancer. *Cancer Cell* **2016**, 30, 474-484.

(15) Stone, L. Kidney cancer: On target - inhibiting SPOP in ccRCC. *Nat. Rev. Urol.* **2016**, 13, 630.

(16) Zheng, T.; Yang, C. G. Targeting SPOP with small molecules provides a novel strategy for kidney cancer therapy. *Sci. China Life Sci.* **2017**, 60, 91-93.

(17) Meanwell, N. A. Synopsis of some recent tactical application of bioisosteres in drug design. *J. Med. Chem.* **2011**, 54, 2529-2591.

(18) St Jean, D. J., Jr.; Fotsch, C. Mitigating heterocycle metabolism in drug discovery. *J. Med. Chem.* **2012**, 55, 6002-6020.

(19) Dhar, A. K.; Mahesh, R.; Jindal, A.; Devadoss, T.; Bhatt, S. Design, synthesis, and pharmacological evaluation of novel 2-(4-substituted piperazin-1-yl)1, 8 naphthyridine 3-carboxylic acids as 5-HT3 receptor antagonists for the management of depression. *Chem. Biol. Drug Des.* **2014**, 84, 721-731.

(20) Manera, C.; Saccomanni, G.; Adinolfi, B.; Benetti, V.; Ligresti, A.; Cascio, M. G.; Tuccinardi, T.; Lucchesi, V.; Martinelli, A.; Nieri, P.; Masini, E.; Di Marzo, V.; Ferrarini, P. L. Rational design, synthesis, and pharmacological properties of new 1,8-naphthyridin-2(1H)-on-3-carboxamide derivatives as highly selective cannabinoid-2 receptor agonists. *J. Med. Chem.* **2009**, 52, 3644-3651.

(21) Bruce, D.; Cardew, E.; Freitag-Pohl, S.; Pohl, E. How to stabilize protein: stability screens for thermal shift assays and nano differential scanning fluorimetry in the virus-X project. *J. Vis. Exp.* **2019**, 144, e58666.

(22) Pai, M. Y.; Lomenick, B.; Hwang, H.; Schiestl, R.; McBride, W.; Loo, J. A.; Huang, J. Drug affinity responsive target stability (DARTS) for small-molecule target identification. *Methods Mol. Biol.* **2015**, 1263, 287-298.

Table of Contents graphic.

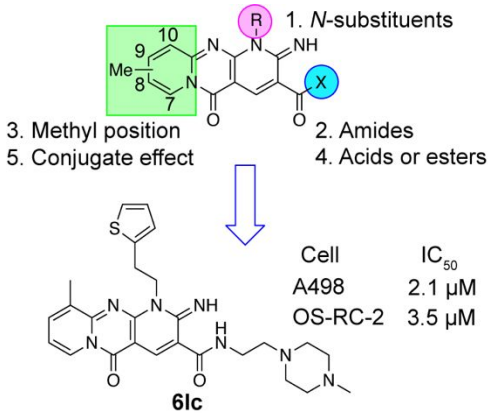

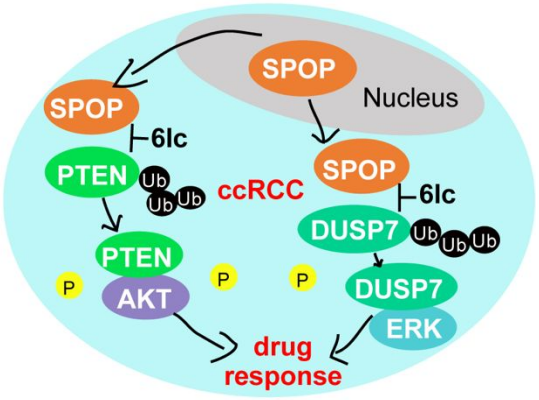

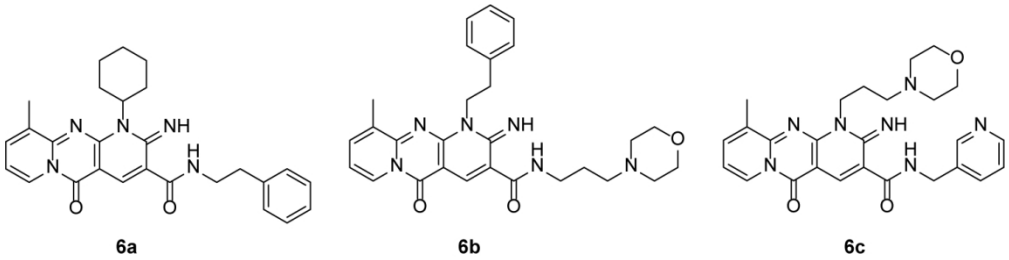

Figure 1

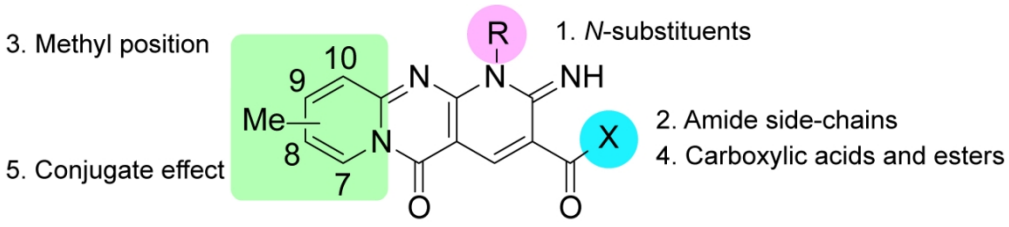
3. Methyl position
5. Conjugate effect
1. N-substituents
2. Amide side-chains
4. Carboxylic acids and esters
R
X
Me
NH
O
O

Figure 2

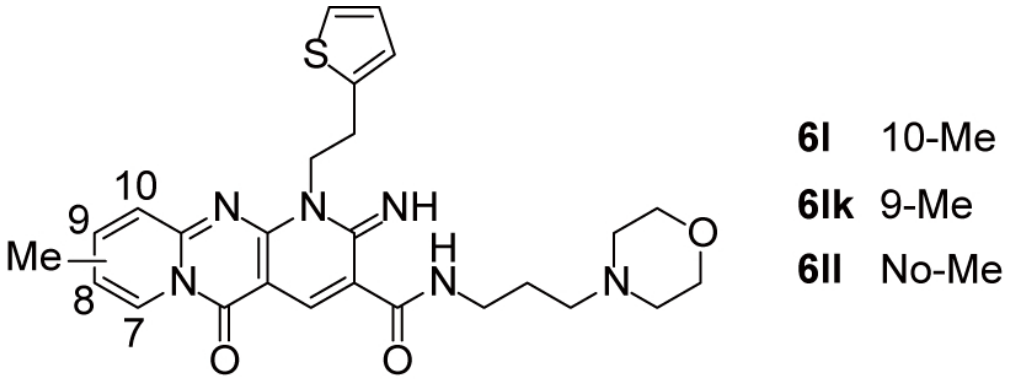

Figure 3

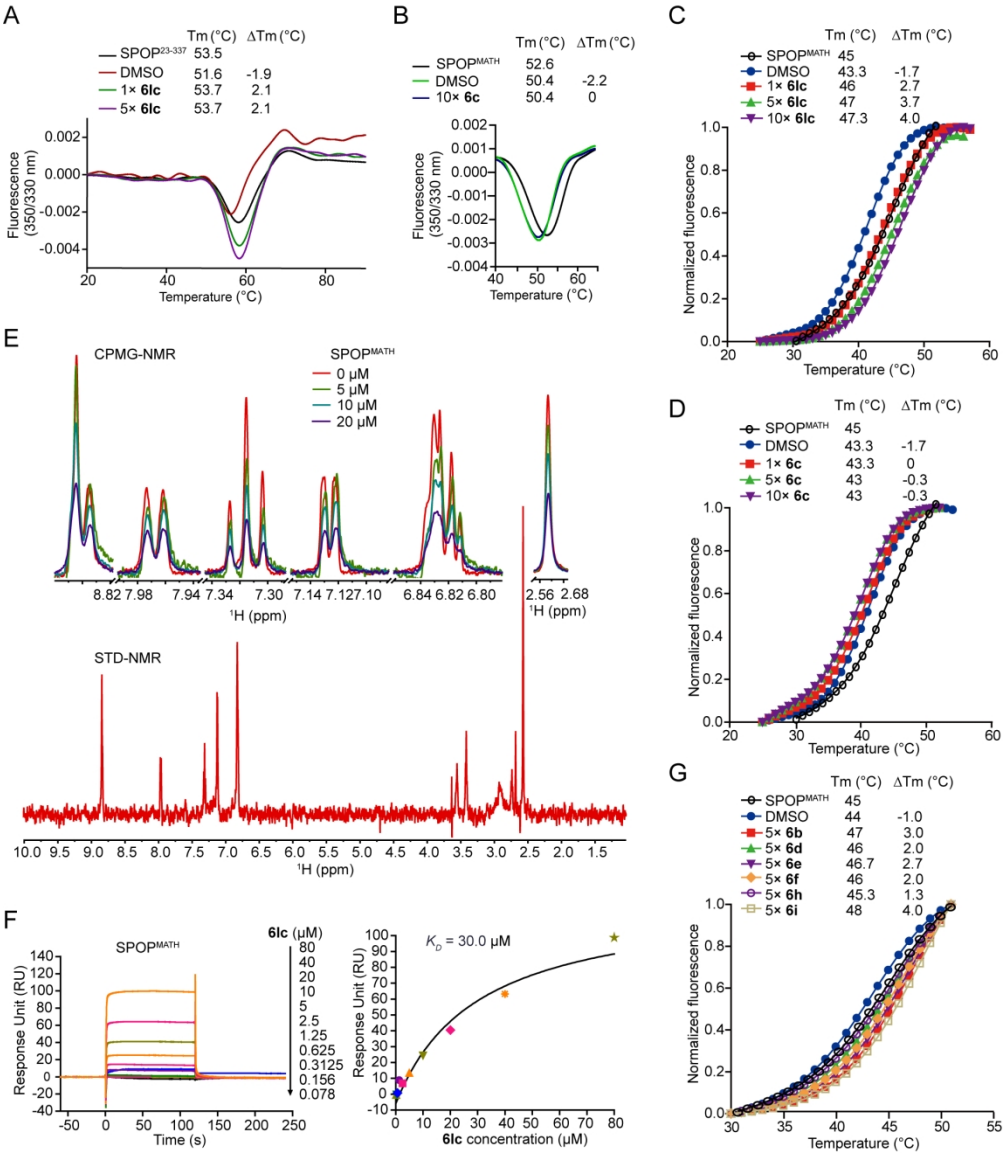
A
Tm (°C) ΔTm (°C)
SPOP23-337 53.5
DMSO 51.6 -1.9
1× 6lc 53.7 2.1
5× 6lc 53.7 2.1
Fluorescence (350/330 nm)
Temperature (°C)
B
Tm (°C) ΔTm (°C)
SPOPMATH 52.6
DMSO 50.4 -2.2
10× 6c 50.4 0
Fluorescence (350/330 nm)
Temperature (°C)
C
Tm (°C) ΔTm (°C)
SPOPMATH 45
DMSO 43.3 -1.7
1× 6lc 46 2.7
5× 6lc 47 3.7
10× 6lc 47.3 4.0
Normalized fluorescence
Temperature (°C)
D
Tm (°C) ΔTm (°C)
SPOPMATH 45
DMSO 43.3 -1.7
1× 6c 43.3 0
5× 6c 43 -0.3
10× 6c 43 -0.3
Normalized fluorescence
Temperature (°C)
E
CPMG-NMR
SPOPMATH
0 μM
5 μM
10 μM
20 μM
8.82 7.98 7.94 7.34 7.30 7.14 7.12 7.10 6.84 6.82 6.80
2.56 2.68
1H (ppm)
STD-NMR
10.0 9.5 9.0 8.5 8.0 7.5 7.0 6.5 6.0 5.5 5.0 4.5 4.0 3.5 3.0 2.5 2.0 1.5
1H (ppm)
F
SPOPMATH
6lc (μM)
80
40
20
10
5
2.5
1.25
0.625
0.3125
0.156
0.078
Response Unit (RU)
Time (s)
KD = 30.0 μM
Response Unit (RU)
6lc concentration (μM)
G
Tm (°C) ΔTm (°C)
SPOPMATH 45
DMSO 44 -1.0
5× 6b 47 3.0
5× 6d 46 2.0
5× 6e 46.7 2.7
5× 6f 46 2.0
5× 6h 45.3 1.3
5× 6i 48 4.0
Normalized fluorescence
Temperature (°C)

Figure 4

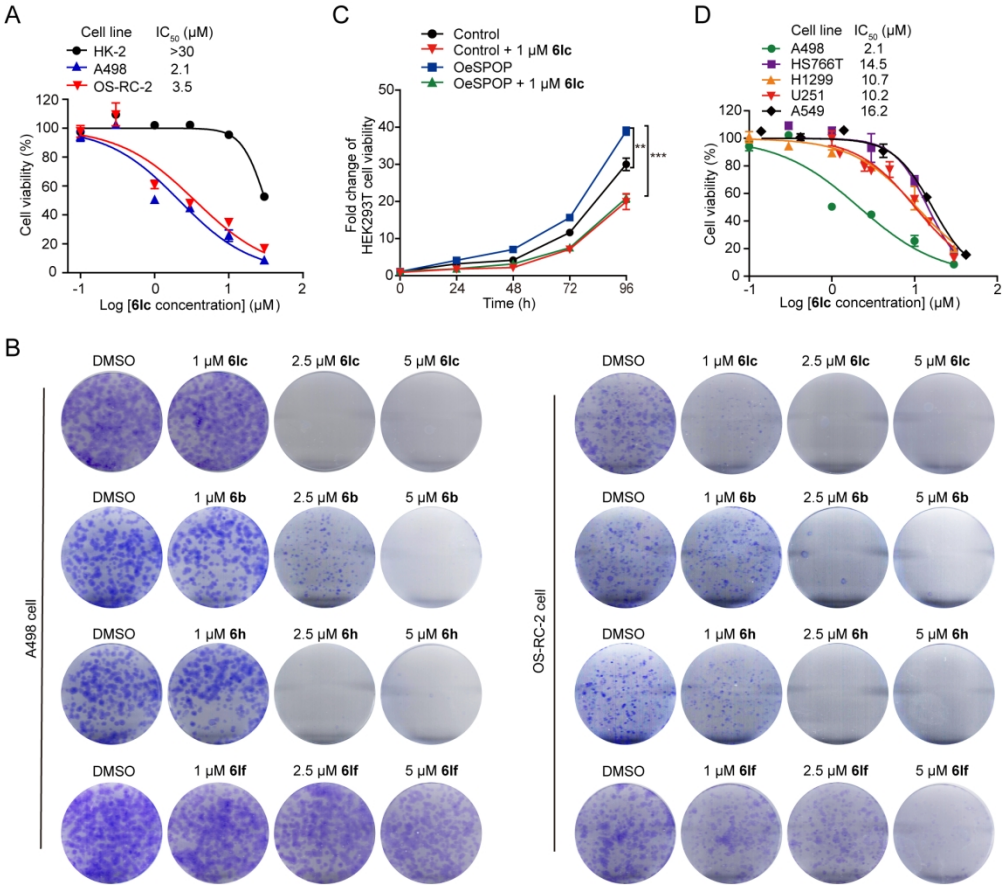
A
Cell line IC50 (μM)
HK-2 >30
A498 2.1
OS-RC-2 3.5
Cell viability (%)
Log [6lc concentration] (μM)
C
Control
Control + 1 μM 6lc
OeSPOP
OeSPOP + 1 μM 6lc
Fold change of HEK293T cell viability
Time (h)
**
***
D
Cell line IC50 (μM)
A498 2.1
HS766T 14.5
H1299 10.7
U251 10.2
A549 16.2
Cell viability (%)
Log [6lc concentration] (μM)
B
DMSO
1 μM 6lc
2.5 μM 6lc
5 μM 6lc
1 μM 6b
2.5 μM 6b
5 μM 6b
1 μM 6h
2.5 μM 6h
5 μM 6h
1 μM 6lf
2.5 μM 6lf
5 μM 6lf
A498 cell
OS-RC-2 cell

Figure 5

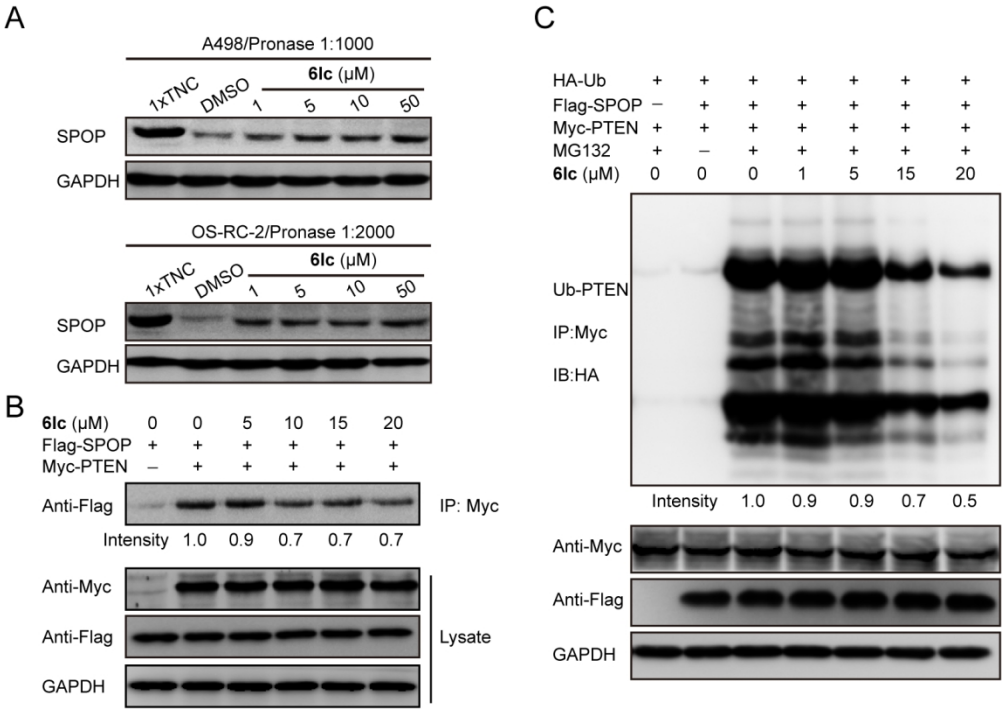
A
A498/Pronase 1:1000
1xTNC
DMSO
6Ic (μM)
1
5
10
50
SPOP
GAPDH
OS-RC-2/Pronase 1:2000
1xTNC
DMSO
6Ic (μM)
1
5
10
50
SPOP
GAPDH
B
6Ic (μM) 0 0 5 10 15 20
Flag-SPOP + + + + + +
Myc-PTEN – + + + + +
Anti-Flag
IP: Myc
Intensity 1.0 0.9 0.7 0.7 0.7
Anti-Myc
Anti-Flag
Lysate
GAPDH
C
HA-Ub + + + + + + +
Flag-SPOP – + + + + + +
Myc-PTEN + + + + + + +
MG132 + – + + + + +
6Ic (μM) 0 0 0 1 5 15 20
Ub-PTEN
IP:Myc
IB:HA
Intensity 1.0 0.9 0.9 0.7 0.5
Anti-Myc
Anti-Flag
GAPDH

Figure 6

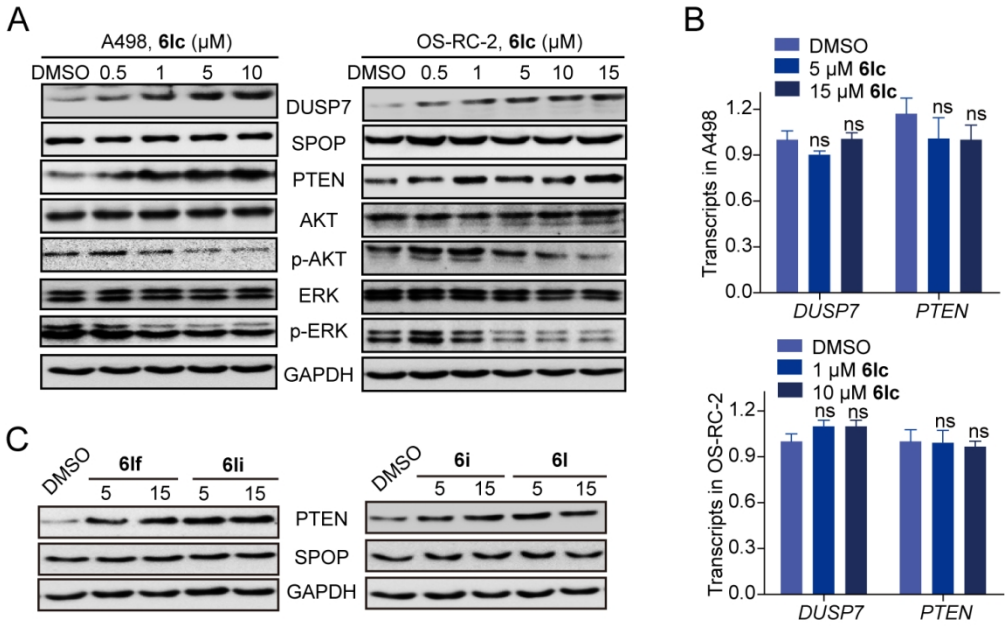
A
A498, 6Ic (μM)
DMSO 0.5 1 5 10
OS-RC-2, 6Ic (μM)
DMSO 0.5 1 5 10 15
DUSP7
SPOP
PTEN
AKT
p-AKT
ERK
p-ERK
GAPDH
B
DMSO
5 μM 6Ic
15 μM 6Ic
Transcripts in A498
1.2
0.9
0.6
0.3
0.0
ns
DUSP7
PTEN
DMSO
1 μM 6Ic
10 μM 6Ic
Transcripts in OS-RC-2
C
DMSO
6If
6Ii
5 15 5 15
DMSO
6i
6I
5 15 5 15
PTEN
SPOP
GAPDH

Figure 7

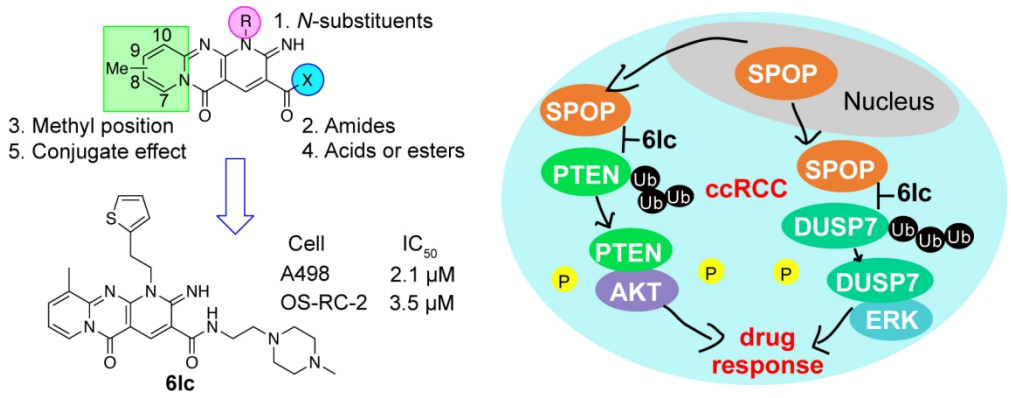

Table of Contents graphic